

Design, Synthesis, and Biological Evaluation of Novel Chromanone Derivatives as Multi-functional Agents for the Treatment of Alzheimer's Disease

Xinnan Li^{a,#}, Tiantian Li^{b,#}, Feiyan Zhan^{a,#}, Feiyue Cheng^b, Li Lu^b, Bocheng Zhang^b, Junda Li^a, Zhaoxin Hu^a, Shengnan Zhou^a, Yilin Jia^a, Stephanie Allen^b, Lisa White^b, James Phillips^c, Zheyong Zhu^{b,*}, Jinyi Xu^{a,*}, Hequan Yao^{a,*}

^a State Key Laboratory of Natural Medicines and Department of Medicinal Chemistry, China Pharmaceutical University, 24 Tong Jia Xiang, Nanjing 210009, P. R. China

^b School of Pharmacy, The University of Nottingham, University Park Campus, Nottingham NG7 2RD, UK

^c School of Pharmacy, University of College London, London WC1N 1AX, UK

AUTHOR INFORMATION

Corresponding Authors

*E-mail: Zheyong.Zhu@nottingham.ac.uk (for Z.Z.)

*E-mail: jinyixu@china.com (for J.X.)

*E-mail: cpuhyao@126.com (for H.Y.)

Author Contributions

[#]X.L. T.L. and F.Z. contributed equally to this work.

ABSTRACT

Based on a multitarget strategy, a series of novel chromanone–1-benzyl-1,2,3,6-tetrahydropyridin hybrids were identified for the potential treatment of Alzheimer's disease (AD). Biological evaluation demonstrated that these hybrids exhibited significant inhibitory activities toward acetylcholinesterase (AChE) and monoamine oxidase B (MAO-B). The optimal compound **C10** possessed excellent dual AChE/MAO-B inhibition both in terms of potency and equilibrium (AChE: $IC_{50} = 0.58 \pm 0.05$

μM ; MAO-B: $\text{IC}_{50} = 0.41 \pm 0.04 \mu\text{M}$). Further molecular modeling and kinetic investigations revealed that compound **C10** was a dual-binding inhibitor bound to both the catalytic anionic site (CAS) and peripheral anionic site (PAS) of AChE. In addition, compound **C10** exhibited low neurotoxicity and potently inhibited AChE enzymatic activity. Furthermore, compound **C10** more effectively protected against mitochondrial dysfunction and oxidation than donepezil, strongly inhibited AChE-induced amyloid aggregation, and moderately reduced glutaraldehyde-induced phosphorylation of tau protein in SH-SY5Y cells. Moreover, compound **C10** displayed largely enhanced improvements in cognitive behaviors and spatial memory in scopolamine-induced AD mice model with better efficacy than donepezil. Overall, the multifunctional profiles of compound **C10** suggest that it deserves further investigation as a promising lead for the prospective treatment of AD.

KEYWORDS: *Chromanone, Monoamine oxidase B, Acetylcholinesterase, Alzheimer's disease, Hybrids.*

INTRODUCTION

Alzheimer's disease (AD), with pathological symptoms of memory loss and other cognitive impairments, is currently one of the most challenging diseases being treated.¹⁻⁴ Over the decades, researchers have presented various hypotheses about the pathogenesis of AD,¹ such as the cholinergic hypothesis,^{5, 6} amyloid cascade hypothesis,⁷⁻⁹ oxidative stress hypothesis,¹⁰⁻¹³ and tau protein hypothesis.^{14, 15} The cholinergic hypothesis is the most recognized and forms an important basis for current therapeutic interventions. The cholinergic neurotransmitter, acetylcholine, is an important chemical substance in the brain. The reduction of cholinergic neurons in the brains of AD patients leads to a decrease in the synthesis, storage and release of acetylcholine, which in turn leads to a series of clinical disorders focusing on memory and recognition dysfunction symptoms.¹⁶ So far, based on the cholinergic hypothesis, the American Food and Drug Administration (FDA) has approved a total of four drugs for clinical use, including tacrine, donepezil, rivastigmine, and galantamine (Figure 1A),

of which tacrine was withdrawn from the market due to its liver toxicity.^{17, 18}

As the crystal structure of the complex between acetylcholinesterase (AChE) and its inhibitor is continuously being resolved, researchers are increasingly able to understand the relationship between the function and structure of AChE at the atomic level, which provides a valuable reference for rationally designing novel drug candidates.¹⁶ The crystal structure of AChE reveals that its active pocket is a narrow “gorge” extending inwards from the surface of the enzyme. At the bottom of the canyon, negatively charged amino acid residues such as Gly199, Trp84, Phe330, and Tyr442 form catalytic anionic site (CAS). Near the entrance of the canyon, there are some negatively charged amino acid residues (Tyr70, Tyr121, Trp279, Asp72, Tyr 334), which together constitute the peripheral anion site (PAS).¹⁹ Studies have shown that there is a close relationship between AChE and amyloid- β ($A\beta$) aggregation, revealing a non-cholinergic function of AChE. The PAS site of AChE binds free $A\beta$ through electrostatic attraction and induces a configurational transformation in the $A\beta$ fibril to β sheet, which accelerates the aggregation of $A\beta$, and further forms the $A\beta$ -AChE complex, which in turn induces a series of biochemical reactions. This leads to dysfunction and apoptosis of nerve cells. Thus, AChE inhibitors acting on PAS sites can inhibit the storage and aggregation of $A\beta$.^{20, 21}

In recent years, in addition to AChE inhibitors, monoamine oxidase B (MAO-B) inhibitors have also received an increasing interest, due to their role in the treatment of AD.^{1, 22, 23} MAOs are a class of enzymes that can catalyze the oxidative deamination of neuroactive and vasoactive amines.²⁴ The class exists as two different subtypes: MAO-A and MAO-B, which are located in the outer mitochondrial membrane of glial cells, neuronal cells, and other cells, and classified according to substrate specificity.^{25, 26} MAO-A is involved in mental state and depression, while MAO-B accelerates the oxidative deamination of neurotransmitters, leading to increased free radical production, which leads to oxidative stress.²⁷ MAO-B is highly active in the brains of AD patients, leading to increased dopamine metabolism, producing large amounts of hydrogen peroxide which ultimately leads to nerve damage. Thus, inhibition of MAO-B may improve the symptoms of AD patients. Studies have shown that several selective MAO-

B inhibitors such as selegiline and rasagiline (Figure 1B) can delay further neurodegeneration of AD patients.^{28, 29} As such, selective inhibition of MAO-B is also an important approach for the treatment of AD.

With the continuous failure to develop single-target anti-AD drugs in recent years, researchers have realized that the pathogenesis of AD is complex and the various factors involved influence each other, thus forming a disease network. A multi-target-directed ligand (MTDL) strategy targeting the AD pathogenesis network has therefore been developed to treat this multifaceted disease. Based on MTDL drug design strategy, Sterling *et al.* combined the pharmacophores of an AChE inhibitor rivastigmine (Figure 2) and a monoamine oxidase inhibitor rasagiline (Figure 2) into a single molecular entity to obtain a new type of dual AChE and MAO-B inhibitor named ladostigil (Figure 2), which is currently under phase II clinical trials.³⁰

Chromanone, 2,3-dihydro-4H-chromen-4-one, is a structural derivative of flavone. Numerous studies have focused on chromanone analogs because they exhibit various bioactivities.³¹ In order to search for novel MAO-B inhibitors, the chromanone structure has been utilized as a promising principal scaffold.³²⁻³⁷ Kong *et al.* reported a series of chromanone derivatives as MAO-B inhibitors, among which compound **5** (Figure 3) showed the best MAO-B inhibitory activity ($IC_{50} = 8.62$ nM).³⁸ Furthermore, many studies have indicated that both chromanone and synthesized analogs showed good MAO-B inhibitory activities.³⁹⁻⁴¹ Recently, we reported an isochromanone derivative (Figure 3) as a potential AChE inhibitor for the treatment of AD.⁴²

On the basis of the evidences that AChE inhibitors are the cornerstone of treatment for AD nowadays and MAO-B inhibitors might represent an alternative approach to treat cognitive dysfunction, the MTDLs combining the inhibition of AChE and MAO-B simultaneously may offer a promising approach for the treatment of AD. In order to search for novel MTDLs, we incorporated the pharmacophores of the AChE inhibitor, donepezil, and the MAO-B inhibitor, chromanone derivative **5**, to a single molecular entity (**C1~C12**, **D1~D8**, Figure 4) with the aim to possess multi-functional properties including inhibition of AChE, anti- $A\beta$ aggregation, inhibition of MAO-B, inhibition of mitochondrial dysfunction and thus reduced levels of reactive oxygen species (ROS).

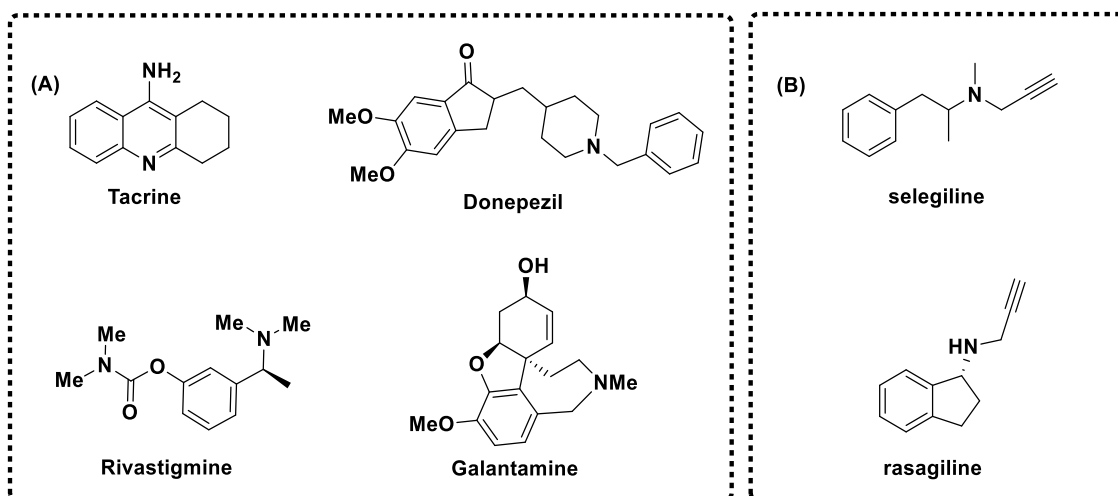


Figure 1. (A) FDA-approved AChE inhibitors for the treatment of AD; (B) The structure of MAO-B inhibitors selegiline and rasagiline

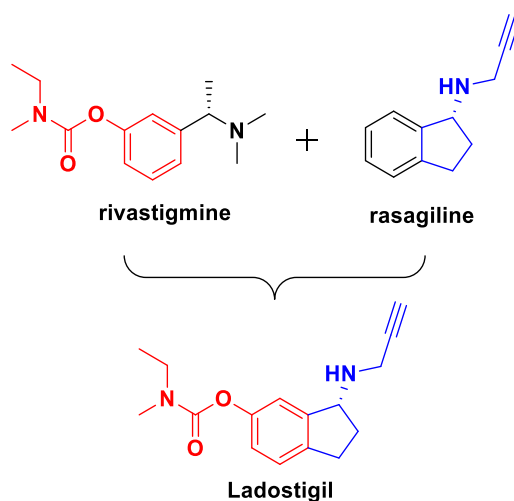


Figure 2. The design of dual AChE & MAO-B inhibitor ladostigil

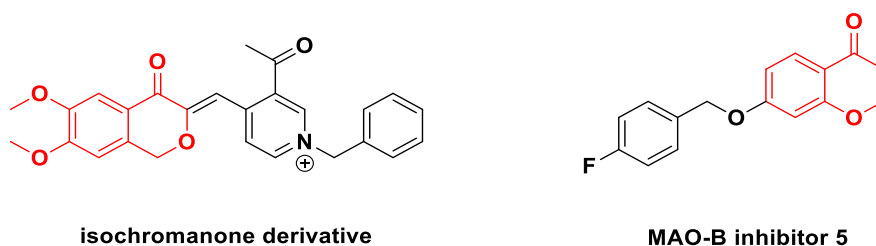


Figure 3. The structure of an isochromanone derivative and MAO-B inhibitor 5.

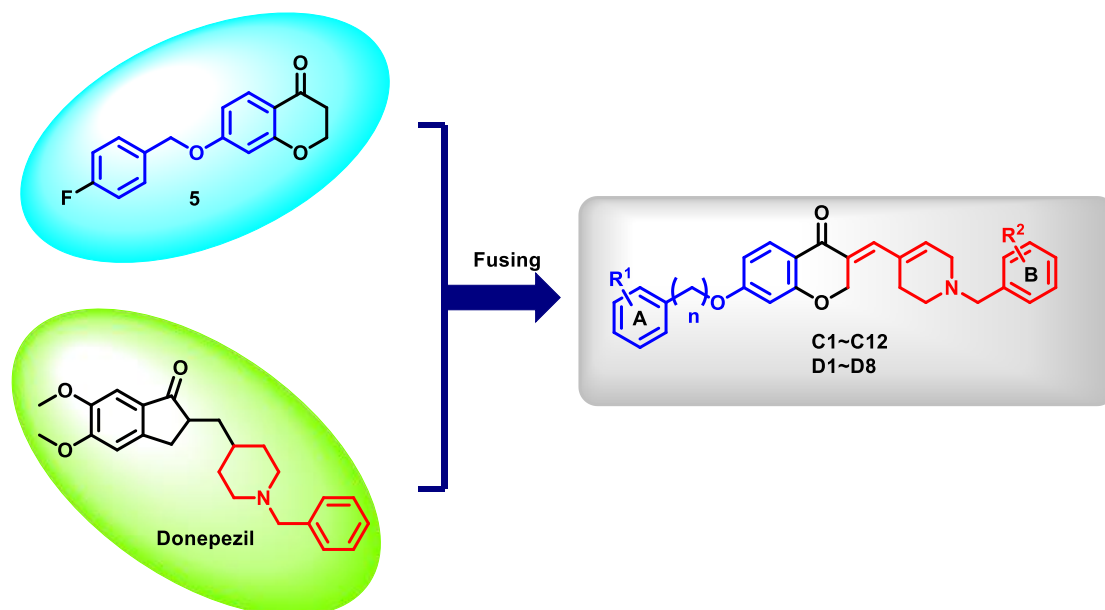
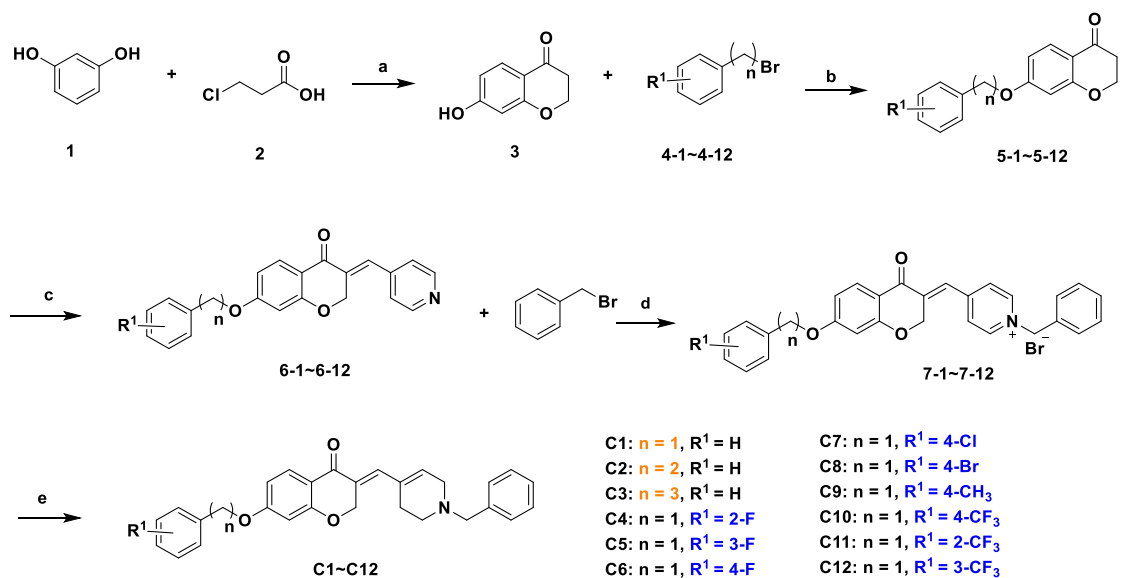


Figure 4. The design of novel dual AChE/MAO-B inhibitors **C1-C12** and **D1-D8**

RESULTS AND DISCUSSION

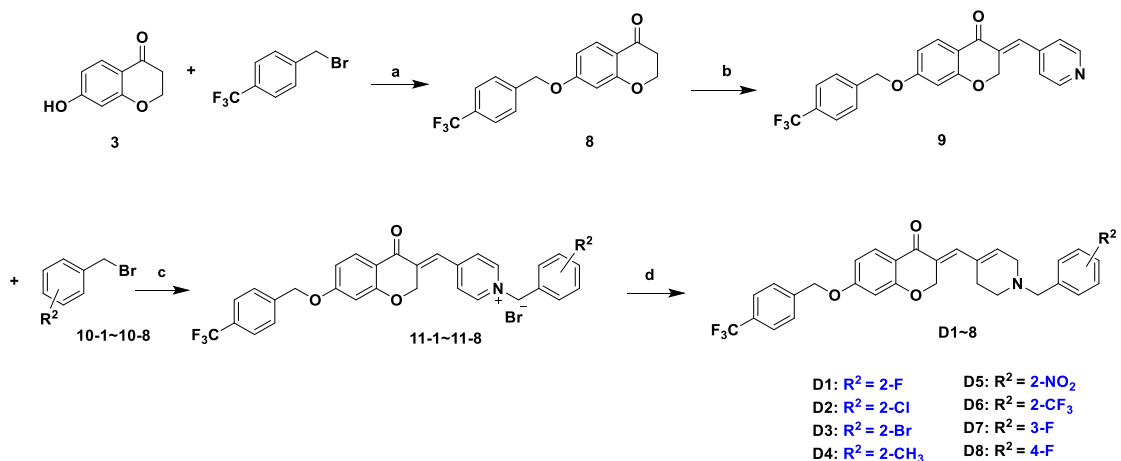
Chemistry. The synthesis protocol for the target compounds **C1-C12** were depicted in Scheme 1. We used commercially available catechol **1** as the starting material, and carried out a substitution reaction with chloropropionic acid **2** under the action of trifluoromethanesulfonic acid, and then carried out cyclization under the action of 2 M NaOH solution. Intermediate **3** was obtained after acidification. After intermediate **3** reacted with the differently substituted compounds **4**, various substituted intermediates **5** were obtained. Intermediate **5** and 4-pyridinecarboxaldehyde underwent aldol condensation to obtain intermediate **6**. Intermediate **6** and benzyl bromide under acetonitrile reflux conditions obtained intermediate **7**, which was then reduced by sodium borohydride to obtain the target compounds **C1-C12**. The synthesis protocol for the target compounds **D1-D8** were depicted in Scheme 2. The synthesis method was basically the same as Scheme 1.

Scheme 1. Synthetic Protocol for the Synthesis of Compounds C1 to C12^a



^aReagents and conditions: (a) 1. CF₃SO₃H, 80 °C, 2 h 2. 2 M NaOH, r.t., 2 h 3. 6 M H₂SO₄, 65% yield; (b) K₂CO₃, DMF, 60 °C, 1 h, 85% yield; (c) Pyridine-4-aldehyde, THF, MeONa, r.t., 2 h, 56% yield; (d) Benzyl bromide, CH₃CN, 2.5 h; (e) NaBH₄, EtOH, - 5 °C, 1 h, 30-70% yield.

Scheme 2. Synthetic Protocol for the Synthesis of Compounds D1 to D8^a



^aReagents and conditions: (a) 4-CF₃-Benzyl bromide, K₂CO₃, DMF, 60 °C, 1 h, 85% yield; (b) Pyridine-4-aldehyde, THF, MeONa, r.t., 2 h, 56% yield; (c) CH₃CN, reflux, 2.5 h; (d) NaBH₄, - 5°C, 1 h, 35 – 45% yield.

Structure activity relationship (SAR) analysis. The AChE inhibitory activity of all target compounds was assessed against *electrophorus electricus* AChE (eeAChE) using

ellman's spectrophotometric method with some minor modifications.^{43, 44} Donepezil was used as the positive control compound. As shown in Table 1, most of the target compounds demonstrated potent inhibitory activity against AChE with IC₅₀ values in the range of sub-micromolar to micromolar.

MAO-B inhibitory activities were explored by measuring the effects on the production of hydrogen peroxide from p-tyramine, according to the reported assay, with pargyline as reference.³⁸ As shown in Table 1, most of the target compounds demonstrated potent inhibitory activity against MAO-B with IC₅₀ values in the sub-micromolar to micromolar range.

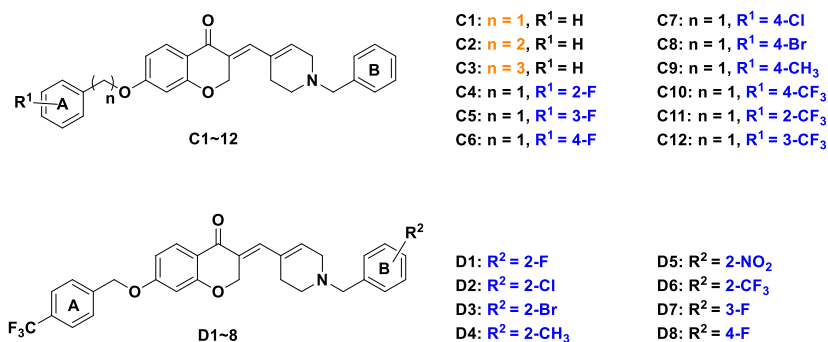
The various structural modifications and activity screening enabled a good comprehension of the structure-activity relationships. The first round of modifications investigated the effect of the length of the link between the A ring and the core, and also the position of the A ring substituents on the activity. The results showed that the shorter the link length, the better the activity. The order of the link length on the activity was found to be $n = 1 > n = 2 > n = 3$ (**C1** > **C2** > **C3**). For inhibitory activity of AChE and MAO-B, the influence on activity of the substitution site of the R¹ group was para- > ortho- > meta- (**C6** > **C4** > **C5**); when the R¹ substituent was a halogen, the inhibitory activity of the compound decreased, and the order of activity was 4-F > 4-Cl > 4-Br (**C6** > **C7** > **C8**). When 4-CH₃ was substituted (**C9**), the inhibitory activity of AChE decreased threefold, and the inhibitory activity of MAO-B remained basically unchanged. When 4-CF₃ was substituted (**C10**), the activity is best and relatively balanced.

In the second round of modifications, we kept $n = 1$, R¹ = 4-CF₃ and investigated the effect of the R² substituent on the B ring. The effect of the position of the R² substituent on the activity of AChE and MAO-B was ortho- > meta- > para- (**D1** > **D7** > **D8**), but the substituents on the B ring were intolerant to activity. When there were substituents on the benzene ring, the inhibitory activity of the compound was also greatly reduced.

After investigations of structural modifications and activity testing, the best compound obtained was **C10** (AChE: IC₅₀ = 0.58 ± 0.05 μM; MAO-B: IC₅₀ = 0.41 ± 0.04 μM), where R¹ is 4-CF₃ substitution, $n = 1$, R² is none; the inhibitory activity of

AChE and MAO-B reached the submicromolar level and the two targets were well balanced.

Table 1. Inhibition of AChE and MAO-B



Compd.	<i>ee</i> AChE IC ₅₀ (μ M) ^a	MAO-B IC ₅₀ (μ M) ^a	Compd.	<i>ee</i> AChE IC ₅₀ (μ M) ^a	MAO-B IC ₅₀ (μ M) ^a
C1	0.68 ± 0.12	0.83 ± 0.18	D1	3.56 ± 1.01	0.92 ± 0.11
C2	4.55 ± 0.65	1.48 ± 0.36	D2	8.42 ± 2.33	1.39 ± 0.45
C3	6.75 ± 1.23	1.52 ± 0.25	D3	> 10	1.85 ± 0.36
C4	2.26 ± 0.12	3.01 ± 0.56	D4	5.56 ± 0.87	4.29 ± 0.89
C5	1.87 ± 0.12	3.85 ± 0.34	D5	> 10	> 10
C6	1.55 ± 0.77	1.01 ± 0.26	D6	> 10	6.65 ± 0.68
C7	2.00 ± 0.89	1.05 ± 0.28	D7	4.74 ± 0.88	3.52 ± 1.12
C8	1.63 ± 0.56	9.93 ± 1.23	D8	5.32 ± 0.92	7.48 ± 1.53
C9	1.82 ± 0.35	0.96 ± 0.78	Donepezil	0.038 ± 0.012	
C10	0.58 ± 0.05	0.41 ± 0.04	Pargyline		0.021 ± 0.005
C11	3.10 ± 0.68	1.55 ± 0.54			
C12	1.25 ± 0.44	3.89 ± 0.57			

^a Results are expressed as the mean of at least three experiments.

Kinetic study of AChE. In order to investigate the mechanism of chromanone derivatives against AChE, an enzyme kinetics study was performed using the representative compound **C10**. The steady-state inhibition data acquired is shown in Figure 5. Lineweaver-Burk reciprocal plots revealed that there was an increasing slope and an increasing intercept at higher inhibitor concentrations, indicating a mixed inhibition mechanism. Based on the kinetic analysis, we concluded that the chromanone

derivatives exhibited as dual binding sites AChE inhibitors, which targeting simultaneously catalytic and peripheral sites of AChE.

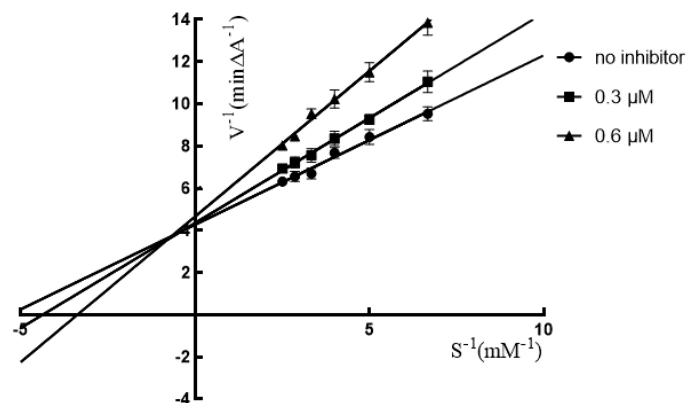


Figure 5. Lineweaver-Burk plot on two distinct concentrations of **C10** for AChE.

Molecular modeling simulations. To gain insights into the binding patterns with the AChE and MAO-B enzymes responsible for the difference in activities, molecular docking simulations were performed using Schrodinger Glide. Structures for AChE and MAO-B, coded as 4EY7 and 2V5Z respectively, were retrieved from the Protein Data Bank (PDB). As shown in Figure 6A/B, compound **C10** is able to occupy the catalytic anionic site (CAS) and the peripheral anionic site (PAS) of AChE. There are five secondary bonds between **C10** and the binding gorge. Among them, the benzene ring of the chromanone fragment forms a π - π interaction with the Trp-286 residue, the pyridine ring forms two π -cations interactions with Tyr-337 and Trp86, the benzyl ring forms a π - π interaction with Trp-86 and the carbonyl group forms a 2.2 Å hydrogen bond with the Phe-295 residue. These results indicate that compound **C10** can simultaneously bind to the PAS and CAS of AChE, which is in accordance with the results of the kinetic study. The binding of **C10** within MAO-B is illustrated in Figure 6C/D, showing that it is fully buried within the enzymatic cavity. the N atom of the pyridine ring forms a 2.2 Å hydrogen bond with the Ile199 residue. Hence, **C10** could fit the binding pockets of both AChE and MAO-B and exhibited good affinity, making it an excellent dual AChE/MAO-B inhibitor.

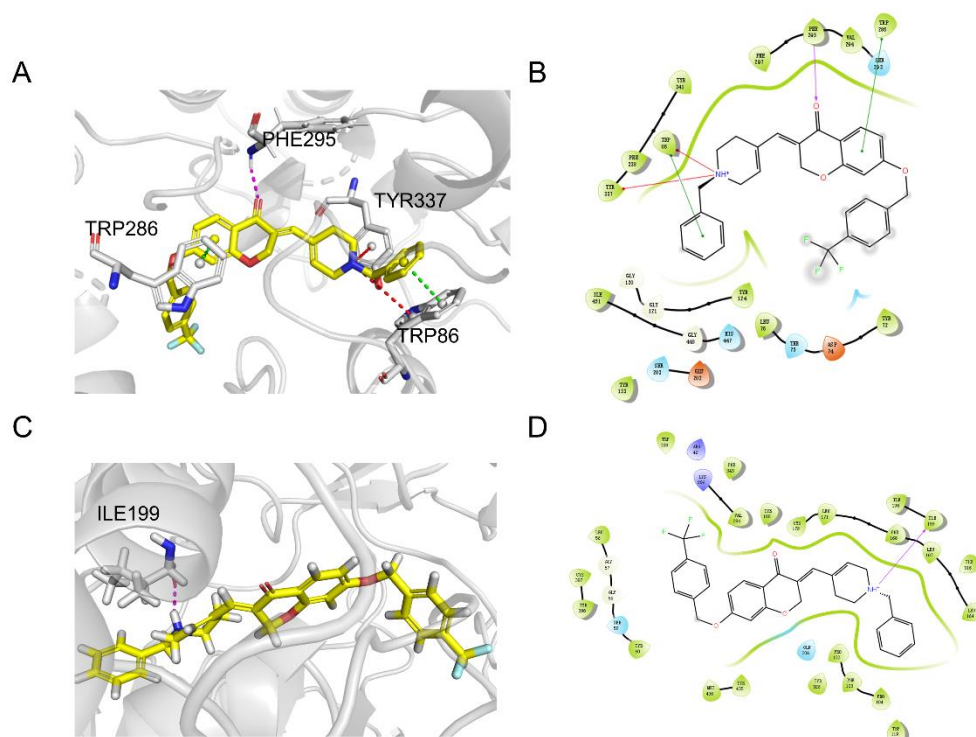


Figure 6. Docking model of compound **C10** with AChE (PDB code: 4EY7) and MAO-B (PDB code: 2V5Z). For secondary bonds, hydrogen bonds are shown as a pink dotted line, the halogen bonds are shown as a pink dotted line, π -cation contacts are shown as green dotted lines, and π - π stacking contacts are shown as green dotted lines. (A) Relative position of compound **C10** in the active pocket of AChE, ligand (**C10**, yellow); the relevant amino acid residues (gray) are rendered as sticks, while the protein is represented as a cartoon (gray). (B) 2D docking interaction plots of **C10** in the AChE active site. (C) Relative position of compound **C10** in the active pocket of MAO-B, ligand (**C10**, yellow); the relevant amino acid residues (gray) are rendered as sticks, while the protein is represented as a cartoon (gray). (D) 2D docking interaction plots of **C10** at the MAO-B active site.

Neurotoxicity studies in SH-SY5Y cells. The neurotoxicity liability of **C10** was evaluated against human neuroblastoma SH-SY5Y cell lines using the 3-(4,5-dimethylthiazol-2-yl)-2,5-diphenyl-tetrazolium bromide (MTT) assay. The results suggested that on exposure to neuroblastoma SH-SY5Y cells compound **C10** exhibited

a nonsignificant reduction in cell viabilities up to the maximum tested concentration of 100 μM (Table 2). The percentage cell viability at the tested concentrations was observed in the range of 96.92-99.58%. The results therefore showed that compound **C10** was not toxic to SH-SY5Y neuroblastoma cells at concentrations up to 100 μM .

Table 2. The neurotoxicity of compound C10 in SH-SY5Y cells

Groups		Cell viability \pm SEM (% control group)		
Control		100.00 \pm 1.06%		
No.	Compound	Final concentration		
		10 μM	50 μM	100 μM
1	C10	99.58 \pm 0.32%	98.18 \pm 0.78%	96.92 \pm 0.66%

AChE inhibition of C10 in SH-SY5Y cells. Inhibitory activity was examined using Ellman's method. Donepezil was used as a positive control. As shown in Figure 7, both **C10** and donepezil effectively inhibit AChE activity at concentrations between 3 μM and 10 μM . At the lower concentrations, between 0.3 μM and 1 μM , the inhibition effect of donepezil is still significant however, **C10** showed only a moderate inhibition effect. These results indicate that compound **C10** has a slightly weaker potency toward intra-cellular AChE inhibition than donepezil.

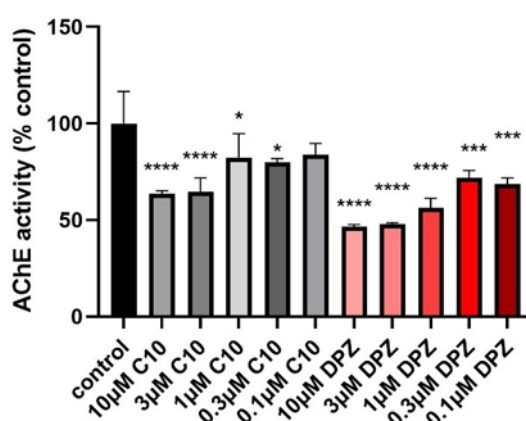


Figure 7. AChE inhibitory effects in SH-SY5Y cells after 24h exposure to different concentrations of **C10**. Activity values are plotted as a percentage of each group divided by the averaged of control, n = 6. P values of statistical significance multiple

comparison tests were analyzed by one-way analysis of variance (ANOVA) followed by Dunnett's test to compare difference between different groups. All data were expressed as means \pm SEM. *P<0.05; **P<0.01; ***P<0.001; ****P<0.0001.

Effects of C10 on AChE-induced A β aggregation. A β aggregation is a critical pathological hallmark of AD. By testing the effects of C10 on amyloid aggregation, the anti-AD potential of C10 can be predicted to some extent. AChE is composed of two binding sites, CAS and PAS. Studies have shown that AChE can play a role in inducing the aggregation of A β and then the formation of amyloid fibrils through the interaction of PAS with A β peptides.⁴⁶ Therefore, the ability of compound C10 to inhibit AChE-induced A β aggregation was tested *in vitro* using the ThT fluorometric assay. As seen in Figure 8, there were significant inhibitory effects of C10 on AChE-induced A β aggregation at applied concentrations between 10 μ M and 0.3 μ M. Moreover, C10 was found to be more potent than donepezil in inhibiting AChE-induced A β aggregation, which might result from dual binding to the CAS and PAS of AChE.

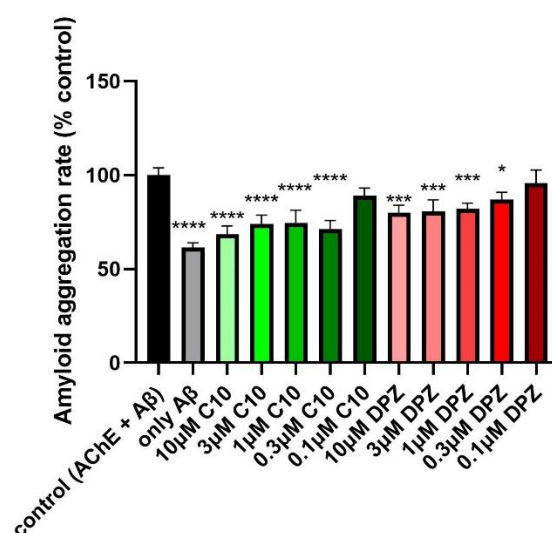


Figure 8. Amyloid aggregation in the presence of AChE when exposed to different concentrations of C10 for 24h. Activity values are plotted as a percentage of each group divided by the averaged of control, n=6. P values of statistical significance multiple comparison tests were analyzed by one-way analysis of variance (ANOVA) followed

by Dunnett's test to compare difference between different groups. All data were expressed as means \pm SEM. * $P < 0.05$; ** $P < 0.01$; *** $P < 0.001$; **** $P < 0.0001$.

Effects of C10 on okadaic-acid (OA)-induced mitochondrial dysfunction. A JC-1 fluorescent assay was used to test the mitochondrial membrane potential (MMP) level in SH-SY5Y cells to investigate whether C10 would protect against OA induced mitochondrial dysfunction. The higher ratio of red to green fluorescence, the higher MMP level, and thus the healthier mitochondrial function. As shown in Figure 9, the ratio of red to green fluorescence is significantly decreased after treatment of SH-SY5Y cells with 30 nM OA for 24 hours compared with the control group. Figure 9 shows that using C10 and donepezil to pre-treat SHSY-5Y cells for 24 hours caused an increase in the red to green fluorescence intensity ratio compared to treatment with OA only. These results demonstrate that OA can induce mitochondrial damage and C10 can effectively protect against this effect, inhibiting MMP levels at the concentrations of 3 μ M and 0.3 μ M. Moreover, C10 shows higher efficacy than donepezil in protecting mitochondrial functions. This enhanced effect of C10 may result from the inhibition of MAO-B.

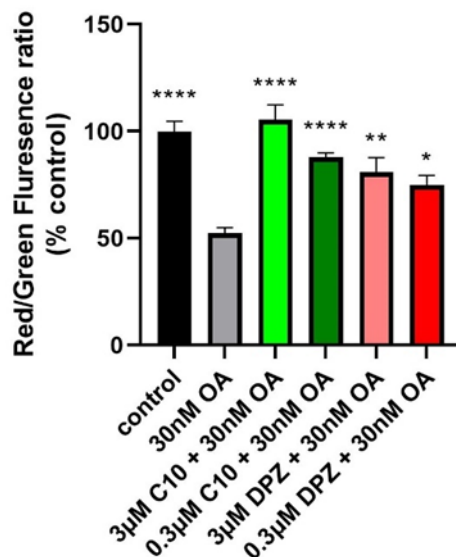


Figure 9. Ratio of red to green fluorescence following JC-1 assay in SH-SY5Y cells exposed to increasing concentrations of C10 prior to exposure to OA for 24h. Activity values are plotted as a percentage of each group divided by the averaged of control,

n=6. P values of statistical significance Multiple comparison tests were analyzed by one-way analysis of variance (ANOVA) followed by Dunnett's test to compare difference between different groups. All data were expressed as means \pm SEM. *P<0.05; **P<0.01; ***P<0.001; ****P<0.0001.

Effects of C10 on OA-induced ROS. A DCF-DA fluorometric assay was used to detect intracellular ROS levels to explore the protective effect of **C10** against OA-induced ROS production. As shown in Figure 10, DCF fluorescence was increased after treatment of SH-SY5Y cells with 30 nM OA for 24 hours compared with the control group. Pre-treatment of these cells with different concentrations of Donepezil and **C10** before exposure to OA caused a reduction in DCF fluorescence intensity compared to the group treated with OA only. These results demonstrate that OA can induce ROS generation, and that **C10** can effectively prevent the generation of intracellular ROS at the applied concentrations of 3 μ M and 0.3 μ M. At the concentration of 3 μ M, **C10** shows a higher degree of protective effect against OA-induced ROS than donepezil. This effect of **C10** may result from the inhibition of MAO-B.

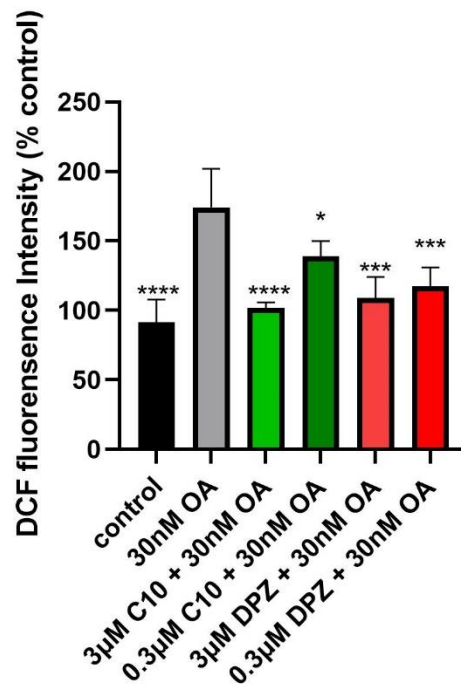


Figure 10. DCF fluorescence intensity in SH-SY5Y cells, pre-treated for 24 hours with increasing concentrations of **C10**, prior to exposure to 30 nM OA for another 24 hours.

Activity values are plotted as a percentage of each group divided by the averaged of control, n=6. P values of statistical significance Multiple comparison tests were analyzed by one-way analysis of variance (ANOVA) followed by Dunnett's test to compare difference between different groups. All data were expressed as means \pm SEM. *P<0.05; **P<0.01; ***P<0.001; ****P<0.0001.

Compound C10 prevents from Glyceraldehyde (GA)-induced phosphorylation of tau protein. Apart from amyloid plaques, another key hallmark of AD pathology is hyperphosphorylation of tau proteins. GA, an inhibitor of glycolysis, results in glycolytic inhibition, cell apoptosis, and an increase in tau protein phosphorylation. Previous studies showed that GA can increase tau phosphorylation in SH-SY5Y cells.^{47, 48} Thus, compound **C10** was tested in SH-SY5Y cells for its ability to inhibit phosphorylation of the tau protein in the neuronal cells using an enzyme-linked immunosorbent assay (ELISA). Donepezil was used as a positive control compound. The results shown in Figure 11 indicate that the phosphorylation ratio of intracellular tau is increased significantly in the 0.7 mM GA treated group compared with the untreated control group. In contrast to the 0.7 mM GA group, compound **C10** presents a significant reduction in p-Tau levels at both the S199 and S396 residues. However, pre-treatment with **C10** (0.3 μ M) for 24 h did not significantly suppress OA-induced hyperphosphorylation of tau protein at both residues. Therefore, compound **C10** was shown to moderately reverse or prevent from GA-induced phosphorylation of tau protein in SH-SY5Y cells.

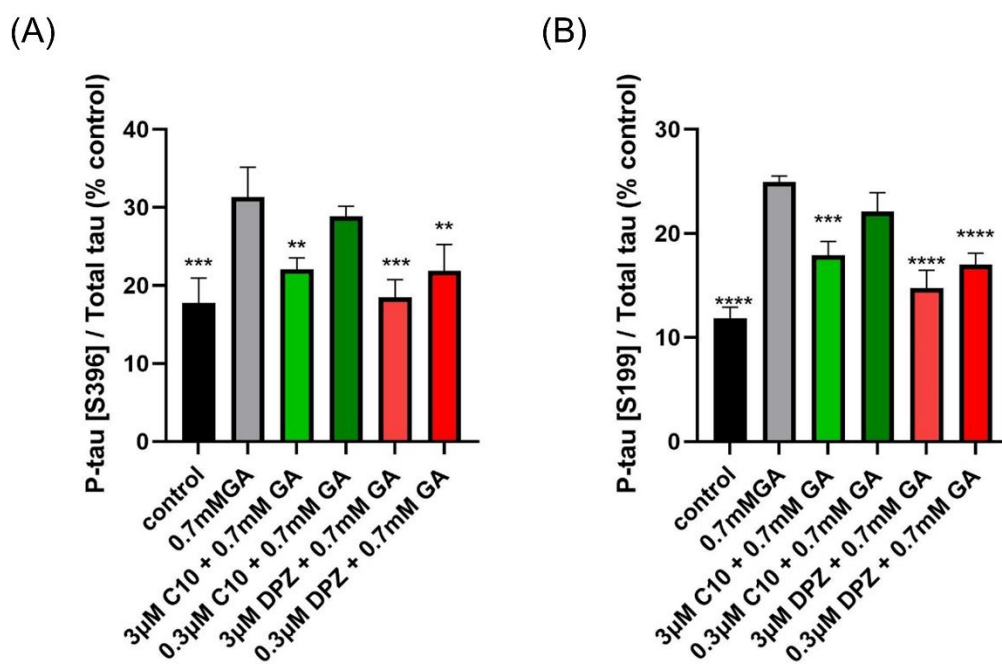


Figure 11. Quantification of phosphorylation ratio of p-Tau/total tau of GA-treated SH-SY5Y cells after C10 or donepezil treatment at 0.3 μ M and 3 μ M. The untreated control group were cells exposed to a vehicle with less than 0.1% DMSO solvent. Tau ratio values are plotted as a percentage of the averaged value derived from vehicle-treated control \pm standard deviation (n=6). Ordinary one-way ANOVA followed by Dunnett's multiple comparisons test were used to compare differences between different groups. *P<0.05; **P<0.01; ***P<0.001; ****P<0.0001. (A) Phosphorylation ratio of p-Tau/total tau on the S396 residue of tau protein. (B) Phosphorylation ratio of p-Tau/total tau on the S199 residue of tau protein.

ADMET prediction of all compounds. The absorption, distribution, metabolism, excretion, and toxicity (ADMET) properties of all compounds were predicted by using ADMET Lab 2.0 (<https://admetmesh.scbdd.com/>), in which compounds with low prediction levels have good ADMET properties. Table S1 shows that most of these compounds likely demonstrate good absorption in the human intestine, moderate blood–brain barrier penetration and clearance. Moreover, the results suggest that most of these compounds are noninhibitors of CYP2C9. Additionally, In AMES and rat acute

toxicity studies, the majority of these compounds were predicted to exhibit no toxicity hazards.

Behavioral Studies in the AD Mice Model. The effects of the optimal compound **C10** on cognitive improvement was assessed in a scopolamine (Scop)-induced amnesia animal model using the Morris water maze (MWM) test; donepezil at 10 mg/kg was used as positive control. Scopolamine can block the cholinergic pathway by antagonizing the muscarinic receptor,⁴⁹ which provides a typical AD model to explore the role of the cholinergic system in cognition and to evaluate anticholinergic drug candidates preclinically.⁵⁰ In this experiment, thirty-two female ICR adult mice were randomly allocated into 4 groups (n = 8 for each group): control, Scop (model), Scop + **C10** (10 mg/kg), Scop + donepezil (10 mg/kg). All mice received 1 training session daily for 4 days before a cognitive ability test. As shown in Figure 12, the Scop group exhibited longer escape latency to target and longer distance to target than the control group (saline-injected group). Compound **C10**, administered to mice by intraperitoneal injection at a dose of 10 mg/kg, rescued the escape latency and distance to target induced by scopolamine, with better effectiveness than donepezil. The effectivity of **C10** for symptom improvement in AD mice model identifies it as a potential lead as an anti-AD agent, especially for the treatment of cholinergic deficiency in the early stage of the disease.

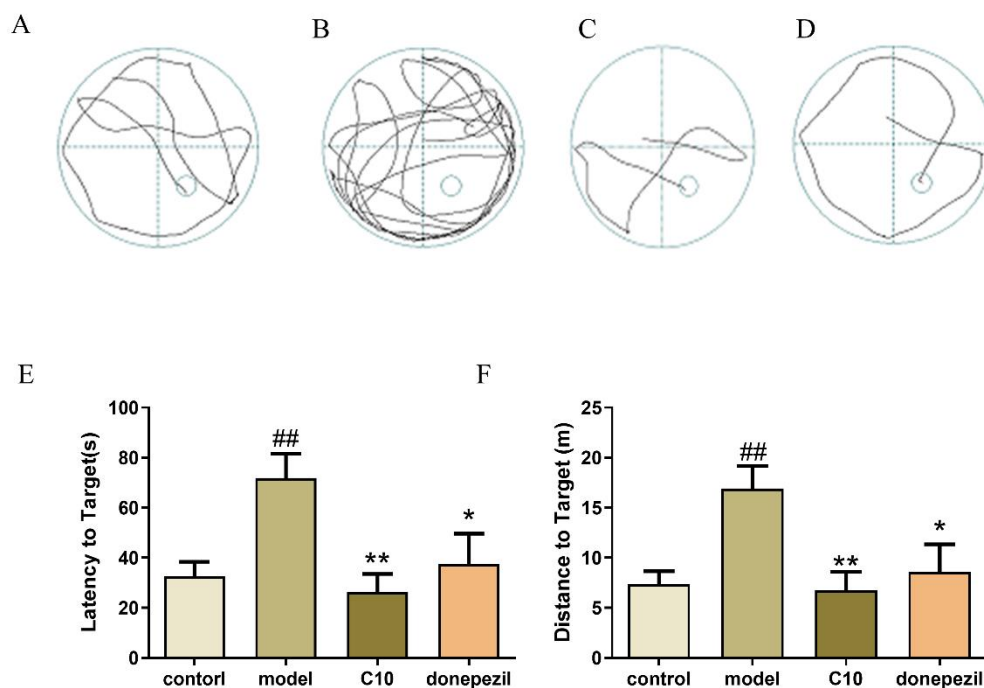


Figure 12. Anti-AD effects of intraperitoneal injection of C10 (10 mg/kg), donepezil (10 mg/kg) on scopolamine-induced cognitive impairment in ICR mice were determined by the Morris water maze test. The trajectories of mice were shown as (A) control, (B) model, (C) C10, (D) donepezil groups, (E) The latency to target, (F) The distance to the target. Data were presented as the mean \pm SEM (n = 8; #p < 0.05, ##p < 0.01, Control group vs. scopolamine model group; *p < 0.05, **p < 0.01, C10 or donepezil group vs. scopolamine model group).

CONCLUSION

As one of the most prevalent neurodegenerative diseases, AD deserves the continued development of novel effective drugs, because of the shortage of disease-modifying or slowing-progression treatments. Due to the complex pathological features of AD, MTDLs may be more advantageous and are becoming an important research direction for the future treatment of AD. In the current work, by fusing the pharmacophores of donepezil and chromanone derivative **5**, a series of novel chromanone-1-benzyl-1,2,3,6-tetrahydropyridin hybrids were designed, synthesized

and evaluated as dual AChE/MAO-B inhibitors. The optimal compound **C10** was found to exhibit no significant cellular neurotoxicity up to the concentration of 100 μ M and inhibited AChE activity up to the concentration of 10 μ M. In addition, compound **C10** was able to more effectively inhibit AChE induced amyloid aggregation than donepezil, and moderately reduce GA-induced phosphorylation of tau protein in SH-SY5Y cells. Furthermore, compound **C10** could more strongly protect against the effects of OA-induced mitochondrial dysfunctions than donepezil, by preventing the decrease of MMP levels and the generation of ROS production. Most importantly, *in vivo* animal studies revealed that compound **C10** significantly ameliorated the cognitive impairment in a scopolamine-induced mice model. All results suggest that compound **C10** is a promising multifunctional lead compound to be further developed as a potential novel drug for AD treatment.

EXPERIMENTAL SECTION

Chemistry. Materials and methods. All starting materials and reference compounds were obtained from commercial sources without further purification. The ^1H NMR and ^{13}C NMR spectra were recorded on a Bruker BioSpin GmbH spectrometer (Bruker, Germany) at (300 or 400) and (75 or 100) MHz respectively, where CDCl_3 or $\text{DMSO-}d_6$ were used as the solvent. Tetramethylsilane was used as standard and chemical shifts are reported in parts per million (ppm), coupling constants J are given in Hertz (Hz), and spin multiplicities are given as singlet (s), broad singlet (br s), doublet (d), doublet of doublets (dd), doublet of doublets of doublets (ddd), triplet (t), doublet of triplets (dt), quartet (q), and multiplet (m). The mass spectrometry (MS, HRMS) data of the compounds were measured using Agilent 1100-LC-MSD-Trap/SL or FTMS-2000 mass spectrometer. The reagents were all commercially available chemically pure or analytical pure products. Solvents were not treated unless otherwise specified use directly. All the reactions were routinely monitored by thin layer chromatography on silica gel and visualized using UV light (254 nm light source). The purity of the representative compounds was $\geq 95\%$, as estimated by HPLC (SHIMADZU Lab solutions, UV detection at $\lambda = 254$ nm) analysis on the Agilent C18 column (4.6×150

mm, 5 mm) eluting at 1 mL/min of menthol and water (95:5).

Synthesis of 7-Hydroxychroman-4-one (3). To a solution of resorcinol (**1**) (1 mmol) in 30 mL trifluoromethanesulfonic acid, 3-chloropropionic acid (1 mmol) was slowly added at 0°C and the mixture was stirred at 80°C for 2 h.³⁸ After the completion of the reaction was detected by TLC, crushed ice was added into the mixture and stirred for another 30 min. And the mixture was extracted with dichloromethane (3 × 100 mL). The combined organic layers were washed with brine (100 mL), dried over anhydrous Na₂SO₄ and purified by flash column chromatography to give white solid **3**. ¹H NMR (300 MHz, DMSO-*d*₆) δ 10.53 (s, 1H), 7.61 (d, *J* = 8.7 Hz, 1H), 6.48 (dd, *J* = 8.7, 2.3 Hz, 1H), 6.30 (d, *J* = 2.3 Hz, 1H), 4.45 (dd, *J* = 6.9, 5.9 Hz, 2H), 2.66 (dd, *J* = 6.8, 5.9 Hz, 2H); ¹³C NMR (75 MHz, DMSO-*d*₆) δ 190.2, 164.8, 163.8, 129.0, 114.4, 110.8, 102.8, 67.4, 37.3; MS(ESI) *m/z*: 165.1 [M + H]⁺.

Synthesis of intermediates 5-1 ~ 5-12. To a solution of 7-Hydroxychroman-4-one (**3**) (1 mmol) and benzyl bromide with different substituted (**4-1** ~ **4-12**) in 10 mL *N,N*-dimethylformamide, potassium carbonate (2 mmol) was added and stirred at 65°C for 2 h.³⁸ After the completion of the reaction was detected by TLC, the mixture was extracted with ethyl acetate (3 × 100 mL). The combined organic layers were washed with brine (200 mL), dried over anhydrous Na₂SO₄ and purified by flash column chromatography to give white solid intermediates **5-1** ~ **5-12**.

Synthesis of intermediates 6-1 ~ 6-12. To a solution of intermediates **5-1** ~ **5-12** (1 mmol) and 4-pyridinecarboxaldehyde (1 mmol) in 20 mL tetrahydrofuran, sodium methoxide (1.5 mmol) was slowly added and the mixture was stirred at room temperature for about 10 min. After the reaction was completed, the mixture was extracted with ethyl acetate (3 × 100 mL). The combined organics were dried over anhydrous Na₂SO₄ and purified by flash column chromatography to give white solid intermediates **6-1** ~ **6-12**.

Synthesis of intermediates 7-1 ~ 7-12. To a solution of intermediates **6-1** ~ **6-12** (1 mmol)

in 10 mL acetonitrile, benzyl bromide (1.1 mmol) was added and the mixture was stirred at 85°C overnight.⁴² After down to room temperature, the mixture was filtered, and the solid collected from this filtration was washed with ethyl acetate for three times. The crude intermediates **7-1** ~ **7-12** were used in the next step without purification.

Synthesis of target compounds C1 ~ C12. To a solution of intermediates **7-1** ~ **7-12** (1 mmol) in 10 mL ethanol, sodium borohydride (0.5 mmol) was added slowly and the mixture was stirred at -5°C for 1 h. After the reaction was completed, the mixture was extracted with ethyl acetate (3 × 100 mL). The combined organics were dried over anhydrous Na₂SO₄ and purified by flash column chromatography to give target compounds **C1** ~ **C12**.

(E)-3-((1-benzyl-1,2,3,6-tetrahydropyridin-4-yl)methylene)-7-(benzyloxy)chroman-4-one (C1). White solid, yield 45.2%. mp:98-99°C. ¹H NMR (300 MHz, CDCl₃) δ 8.13 (d, *J* = 8.9 Hz, 1H), 7.69 (s, 1H), 7.47 – 7.26 (m, 10H), 7.03 (dd, *J* = 8.9, 2.3 Hz, 1H), 6.88 (d, *J* = 2.2 Hz, 1H), 5.47 (s, 1H), 5.15 (s, 2H), 3.63 (s, 2H), 3.15 (s, 2H), 3.03 (s, 2H), 2.62 (s, 2H), 2.19 (s, 2H); ¹³C NMR (75 MHz, CDCl₃) δ 162.8, 158.1, 158.0, 157.9, 152.8, 137.4, 135.7, 133.7, 129.3, 128.7, 128.3, 128.2, 127.5, 127.2, 125.2, 121.9, 120.95, 114.8, 101.1, 70.4, 62.4, 52.5, 49.5, 31.9, 28.7. MS(ESI) *m/z*: 438.2 [M + H]⁺.

(E)-3-((1-benzyl-1,2,3,6-tetrahydropyridin-4-yl)methylene)-7-phenethoxychroman-4-one (C2). White solid, yield 50.6%. mp:101-103°C. ¹H NMR (400 MHz, Chloroform-*d*) δ 8.11 (d, *J* = 8.9 Hz, 1H), 7.75 (s, 1H), 7.43 (d, *J* = 6.8 Hz, 2H), 7.35 (d, *J* = 3.7 Hz, 2H), 7.34 (s, 1H), 7.32 (d, *J* = 4.1 Hz, 2H), 7.30 (s, 2H), 7.28 – 7.25 (m, 1H), 6.96 (dd, *J* = 8.9, 2.4 Hz, 1H), 6.81 (d, *J* = 2.4 Hz, 1H), 5.48 (dd, *J* = 3.3, 1.7 Hz, 1H), 4.26 (t, *J* = 7.0 Hz, 2H), 3.74 (s, 2H), 3.17 (d, *J* = 2.4 Hz, 2H), 3.15 (d, *J* = 7.1 Hz, 2H), 3.14 – 3.11 (m, 2H), 2.74 (t, *J* = 5.8 Hz, 2H), 2.26 (d, *J* = 6.2 Hz, 2H); ¹³C NMR (75 MHz, Chloroform-*d*) δ 177.03, 163.10, 158.23, 153.01, 137.63, 135.57, 134.07, 129.81, 129.02, 128.63, 128.52, 127.87, 127.26, 126.77, 121.60, 119.68, 117.74, 114.83, 100.68,

69.24, 61.63, 51.77, 49.22, 35.49, 32.10, 28.03. MS(ESI) m/z : 452.2 [M + H]⁺.

(E)-3-((1-benzyl-1,2,3,6-tetrahydropyridin-4-yl)methylene)-7-(3-phenylpropoxy)chroman-4-one (**C3**). White solid, yield 44.5%. mp:108-110°C. ¹H NMR (300 MHz, CDCl₃) δ 8.11 (d, J = 8.9 Hz, 1H), 7.70 (s, 1H), 7.26 (s, 7H), 7.21 (dt, J = 8.8, 3.0 Hz, 3H), 6.95 (dd, J = 8.9, 2.3 Hz, 1H), 6.76 (d, J = 2.4 Hz, 1H), 5.47 (dt, J = 3.6, 2.0 Hz, 1H), 4.02 (t, J = 6.2 Hz, 2H), 3.64 (s, 2H), 3.15 (s, 2H), 3.09 – 2.99 (m, 2H), 2.83 (t, J = 7.5 Hz, 2H), 2.64 (t, J = 5.8 Hz, 2H), 2.26 – 2.09 (m, 4H). ¹³C NMR (75 MHz, CDCl₃) δ 177.07, 163.30, 158.25, 152.80, 141.09, 137.79, 133.78, 129.38, 128.55, 128.29, 127.36, 127.21, 126.15, 121.96, 121.19, 117.77, 114.76, 100.61, 67.49, 62.51, 52.62, 49.66, 32.09, 32.04, 30.53, 28.93. MS(ESI) m/z : 466.2 [M + H]⁺.

(E)-3-((1-benzyl-1,2,3,6-tetrahydropyridin-4-yl)methylene)-7-((2-fluorobenzyl)oxy)chroman-4-one (**C4**). White solid, yield 48.2%. mp:94-95°C. ¹H NMR (300 MHz, CDCl₃) δ 8.14 (d, J = 9.0 Hz, 1H), 7.68 (s, 1H), 7.50 (td, J = 7.5, 1.8 Hz, 1H), 7.40 – 7.28 (m, 5H), 7.26 – 7.08 (m, 3H), 7.03 (dd, J = 8.9, 2.4 Hz, 1H), 6.91 (d, J = 2.3 Hz, 1H), 5.47 (t, J = 1.7 Hz, 1H), 5.21 (s, 2H), 3.57 (s, 2H), 3.14 (s, 2H), 3.02 – 2.94 (m, 2H), 2.57 (t, J = 5.7 Hz, 2H), 2.15 (t, J = 3.9 Hz, 2H); ¹³C NMR (75 MHz, CDCl₃) δ 177.0, 162.6, 158.1, 152.8, 133.7, 130.2, 129.8, 129.7, 129.3, 128.3, 127.5, 127.2, 124.5, 124.4, 122.0, 121.2, 118.18, 115.7, 115.4, 114.8, 101.1, 64.2, 62.5, 52.7, 49.7, 32.0, 28.6. MS(ESI) m/z : 456.2 [M + H]⁺.

(E)-3-((1-benzyl-1,2,3,6-tetrahydropyridin-4-yl)methylene)-7-((3-fluorobenzyl)oxy)chroman-4-one (**C5**). White solid, yield 55.6%. mp:93-95°C. ¹H NMR (300 MHz, CDCl₃) δ 8.14 (d, J = 9.0 Hz, 1H), 7.66 (s, 1H), 7.42 – 7.28 (m, 5H), 7.25 – 7.12 (m, 3H), 7.04 (ddd, J = 11.3, 8.5, 2.5 Hz, 2H), 6.85 (d, J = 2.4 Hz, 1H), 5.47 (s, 1H), 5.13 (s, 2H), 3.56 (s, 2H), 3.14 (s, 2H), 2.97 (d, J = 3.4 Hz, 2H), 2.55 (t, J = 5.7 Hz, 2H), 2.14 (d, J = 5.9 Hz, 2H); ¹³C NMR (75 MHz, CDCl₃) δ 176.9, 162.5, 158.0, 152.7, 138.2, 133.6, 130.4, 130.3, 129.2, 128.2, 127.5, 127.0, 122.8, 122.1, 121.4, 115.4,

115.1, 114.7, 114.4, 114.1, 101.2, 69.5, 62.7, 52.8, 49.7, 32.0, 29.1. MS(ESI) m/z : 456.2 [M + H]⁺.

(E)-3-((1-benzyl-1,2,3,6-tetrahydropyridin-4-yl)methylene)-7-((4-fluorobenzyl)oxy)chroman-4-one (**C6**). White solid, yield 65.2%. mp:95-96°C. ¹H NMR (400 MHz, Chloroform-*d*) δ 8.12 (d, J = 8.9 Hz, 1H), 7.71 (s, 1H), 7.43 (d, J = 2.0 Hz, 1H), 7.41 (d, J = 3.1 Hz, 1H), 7.40 – 7.38 (m, 1H), 7.37 – 7.36 (m, 1H), 7.34 – 7.29 (m, 2H), 7.27 (dd, J = 6.7, 1.9 Hz, 1H), 7.12 – 7.06 (m, 2H), 7.01 (dd, J = 8.9, 2.4 Hz, 1H), 6.86 (d, J = 2.4 Hz, 1H), 5.47 (tt, J = 3.4, 1.6 Hz, 1H), 5.09 (s, 2H), 3.66 (s, 2H), 3.15 (s, 2H), 3.09 – 2.99 (m, 2H), 2.65 (t, J = 5.8 Hz, 2H), 2.24 – 2.12 (m, 2H); ¹³C NMR (101 MHz, Chloroform-*d*) δ 176.95, 162.71, 162.71, 158.13, 152.92, 133.88, 131.53, 129.52, 129.43, 128.39, 127.51, 127.46, 121.88, 120.50, 118.06, 115.83, 115.62, 114.86, 101.21, 69.82, 62.13, 52.25, 49.48, 32.07, 28.52. MS(ESI) m/z : 456.2 [M + H]⁺.

(E)-3-((1-benzyl-1,2,3,6-tetrahydropyridin-4-yl)methylene)-7-((4-chlorobenzyl)oxy)chroman-4-one (**C7**). White solid, yield 66.3%. mp:98-100°C. ¹H NMR (300 MHz, CDCl₃) δ 8.13 (d, J = 9.0 Hz, 1H), 7.68 (d, J = 1.0 Hz, 1H), 7.38 (s, 4H), 7.33 (d, J = 1.5 Hz, 2H), 7.31 (d, J = 0.9 Hz, 1H), 7.28 (dd, J = 3.4, 1.5 Hz, 1H), 7.25 (d, J = 0.9 Hz, 1H), 7.01 (dd, J = 8.9, 2.4 Hz, 1H), 6.85 (d, J = 2.4 Hz, 1H), 5.50 – 5.44 (m, 1H), 5.10 (s, 2H), 3.59 (s, 2H), 3.14 (s, 2H), 3.00 (s, 2H), 2.58 (t, J = 5.7 Hz, 2H), 2.16 (s, 2H); ¹³C NMR (75 MHz, Chloroform-*d*) δ 176.97, 162.63, 158.13, 153.04, 134.26, 134.21, 134.03, 129.80, 128.98, 128.86, 128.53, 127.89, 127.46, 121.70, 119.18, 118.06, 114.91, 101.22, 69.69, 61.67, 51.78, 49.23, 32.09, 29.73. MS(ESI) m/z : 472.2 [M + H]⁺.

(E)-3-((1-benzyl-1,2,3,6-tetrahydropyridin-4-yl)methylene)-7-((4-bromobenzyl)oxy)chroman-4-one (**C8**). White solid, yield 68.5%. mp:102-103°C. ¹H NMR (300 MHz, Chloroform-*d*) δ 8.12 (d, J = 8.9 Hz, 1H), 7.70 (s, 1H), 7.53 (d, J =

8.0 Hz, 2H), 7.37 – 7.27 (m, 7H), 7.00 (d, $J = 9.0$ Hz, 1H), 6.84 (s, 1H), 5.46 (s, 1H), 5.08 (s, 2H), 3.62 (s, 2H), 3.14 (s, 2H), 3.02 (s, 2H), 2.61 (t, $J = 5.8$ Hz, 2H). ^{13}C NMR (75 MHz, CDCl_3) δ 177.03, 162.60, 158.13, 152.89, 137.87, 134.81, 133.75, 131.98, 129.37, 129.18, 128.32, 127.62, 127.23, 122.43, 122.10, 121.27, 118.19, 114.85, 101.25, 69.75, 62.62, 52.73, 49.73, 32.10, 29.01. MS(ESI) m/z : 516.1 $[\text{M} + \text{H}]^+$.

(E)-3-((1-benzyl-1,2,3,6-tetrahydropyridin-4-yl)methylene)-7-((4-methylbenzyl)oxy)chroman-4-one (**C9**). White solid, yield 44.3%. mp:110-112°C. ^1H NMR (300 MHz, CDCl_3) δ 8.12 (d, $J = 8.9$ Hz, 1H), 7.68 (s, 1H), 7.38 – 7.27 (m, 7H), 7.22 (d, $J = 7.9$ Hz, 2H), 7.02 (dd, $J = 8.9, 2.4$ Hz, 1H), 6.87 (d, $J = 2.4$ Hz, 1H), 5.47 (s, 1H), 5.10 (s, 2H), 3.62 (s, 2H), 3.15 (s, 2H), 3.02 (s, 2H), 2.61 (s, 2H), 2.37 (s, 3H), 2.17 (s, 2H). ^{13}C NMR (75 MHz, CDCl_3) δ 177.05, 162.97, 158.16, 152.80, 138.32, 138.23, 133.74, 132.71, 129.49, 129.27, 128.26, 127.75, 127.43, 127.09, 122.04, 121.43, 117.96, 114.98, 101.15, 70.49, 62.74, 52.87, 49.80, 32.08, 29.13, 21.30. MS(ESI) m/z : 452.2 $[\text{M} + \text{H}]^+$.

(E)-3-((1-benzyl-1,2,3,6-tetrahydropyridin-4-yl)methylene)-7-((4-(trifluoromethyl)benzyl)oxy)chroman-4-one (**C10**). mp:85-88°C. White solid, yield 36.2%. ^1H NMR (300 MHz, CDCl_3) δ 8.15 (d, $J = 8.9$ Hz, 1H), 7.73 – 7.64 (m, 3H), 7.56 (d, $J = 8.1$ Hz, 2H), 7.40 – 7.24 (m, 5H), 7.03 (dd, $J = 8.9, 2.4$ Hz, 1H), 6.86 (d, $J = 2.4$ Hz, 1H), 5.47 (td, $J = 3.3, 1.6$ Hz, 1H), 5.20 (s, 2H), 3.63 (s, 2H), 3.15 (s, 2H), 3.03 (s, 2H), 2.62 (t, $J = 5.8$ Hz, 2H), 2.18 (s, 2H); ^{13}C NMR (75 MHz, CDCl_3) δ 176.96, 162.42, 158.09, 152.86, 139.84, 138.19, 133.67, 130.74, 130.31, 129.27, 128.27, 127.67, 127.50, 127.11, 125.79, 125.74, 122.16, 121.49, 118.28, 114.74, 101.25, 77.57, 77.14, 76.72, 69.54, 62.73, 52.85, 49.79, 32.06, 29.13. $\text{C}_{30}\text{H}_{26}\text{F}_3\text{NO}_3$, High-resolution mass-MS calculated for m/z $[\text{M} + \text{H}]^+$: 506.1938 (calculated), 506.1947 (found).

(E)-3-((1-benzyl-1,2,3,6-tetrahydropyridin-4-yl)methylene)-7-((2-(trifluoromethyl)benzyl)oxy)chroman-4-one (**C11**). White solid, yield 35.6%. mp:82-

83°C. ¹H NMR (300 MHz, CDCl₃) δ 8.14 (d, *J* = 8.9 Hz, 1H), 7.78 – 7.67 (m, 3H), 7.58 (td, *J* = 7.6, 1.2 Hz, 1H), 7.50 – 7.38 (m, 3H), 7.37 – 7.27 (m, 3H), 7.04 (dd, *J* = 8.9, 2.4 Hz, 1H), 6.87 (d, *J* = 2.4 Hz, 1H), 5.47 (p, *J* = 1.6 Hz, 1H), 5.34 (s, 2H), 3.73 (s, 2H), 3.16 (s, 2H), 3.12 (s, 2H), 2.73 (t, *J* = 5.8 Hz, 2H), 2.27 (d, *J* = 6.3 Hz, 2H); ¹³C NMR (75 MHz, CDCl₃) δ 176.9, 162.3, 158.1, 153.0, 134.2, 134.0, 132.3, 129.7, 128.7, 128.5, 128.2, 127.8, 127.5, 126.2, 126.1, 126.0, 122.4, 121.7, 119.8, 118.2, 114.8, 101.3, 66.6, 61.6, 51.8, 49.2, 32.0, 28.0. MS(ESI) *m/z*: 506.2 [M + H]⁺.

(E)-3-((1-benzyl-1,2,3,6-tetrahydropyridin-4-yl)methylene)-7-((3-(trifluoromethyl)benzyl)oxy)chroman-4-one (**C12**). mp:80-82°C. White solid, yield 52.2%. ¹H NMR (300 MHz, CDCl₃) δ 8.14 (d, *J* = 8.9 Hz, 1H), 7.77 (s, 1H), 7.72 (s, 1H), 7.68 – 7.59 (m, 2H), 7.59 – 7.50 (m, 1H), 7.42 (dd, *J* = 7.8, 1.8 Hz, 2H), 7.38 – 7.28 (m, 3H), 7.04 (dd, *J* = 8.9, 2.4 Hz, 1H), 6.89 (d, *J* = 2.4 Hz, 1H), 5.47 (dt, *J* = 3.3, 1.7 Hz, 1H), 5.18 (s, 2H), 3.74 (s, 2H), 3.16 (s, 2H), 3.15 – 3.07 (m, 2H), 2.73 (t, *J* = 5.8 Hz, 2H), 2.25 (d, *J* = 7.2 Hz, 2H); ¹³C NMR (75 MHz, CDCl₃) δ 176.9, 162.4, 158.1, 153.0, 136.7, 134.0, 131.3, 130.6, 129.7, 129.3, 128.5, 127.8, 127.5, 125.7, 125.2, 125.2, 124.1, 124.1, 121.7, 118.2, 114.8, 101.2, 69.6, 61.7, 51.8, 49.2, 32.0, 28.1. MS(ESI) *m/z*: 506.2 [M + H]⁺.

Synthesis of intermediates 8. The intermediate **8** was synthesized according to the procedure of intermediate **5**.

Synthesis of intermediates 9. The intermediate **9** was synthesized according to the procedure of intermediate **6**.

Synthesis of intermediates 11. The intermediate **11** was synthesized according to the procedure of intermediate **7**.

Synthesis of target compounds B1-B8. The target compounds **B1-B8** was synthesized

according to the procedure of target compounds **A1-A12**.

(E)-3-((1-(2-fluorobenzyl)-1,2,3,6-tetrahydropyridin-4-yl)methylene)-7-((4-(trifluoromethyl)benzyl)oxy)chroman-4-one (**D1**). White solid, yield 40.6%. mp:98-99°C. ¹H NMR (300 MHz, Chloroform-*d*) δ 8.13 (d, *J* = 8.9 Hz, 1H), 7.73 (s, 1H), 7.67 (d, *J* = 8.1 Hz, 2H), 7.56 (d, *J* = 8.0 Hz, 2H), 7.48 (d, *J* = 1.8 Hz, 1H), 7.26 (d, *J* = 5.4 Hz, 2H), 7.15 – 7.09 (m, 1H), 7.08 – 7.04 (m, 1H), 7.02 (dd, *J* = 5.7, 3.2 Hz, 1H), 6.86 (d, *J* = 2.4 Hz, 1H), 5.48 (s, 1H), 5.20 (s, 2H), 3.77 (s, 2H), 3.15 (s, 2H), 3.12 (s, 2H), 2.72 (t, *J* = 5.8 Hz, 2H), 2.24 (t, *J* = 5.4 Hz, 2H); ¹³C NMR (75 MHz, Chloroform-*d*) δ 176.95, 162.45, 158.10, 153.03, 139.78, 133.84, 132.20, 130.74, 129.60, 127.59, 127.46, 125.77, 125.72, 124.22, 122.21, 121.81, 120.22, 118.19, 115.50, 115.19, 114.79, 101.25, 69.53, 54.09, 51.63, 49.29, 32.04, 29.72. MS(ESI) *m/z*: 524.2 [M + H]⁺.

(E)-3-((1-(2-chlorobenzyl)-1,2,3,6-tetrahydropyridin-4-yl)methylene)-7-((4-(trifluoromethyl)benzyl)oxy)chroman-4-one (**D2**). White solid, yield 41.5%. mp:102-104°C. ¹H NMR (300 MHz, Chloroform-*d*) δ 8.16 (d, *J* = 8.9 Hz, 1H), 7.72 (s, 1H), 7.68 (d, *J* = 8.1 Hz, 2H), 7.59 (s, 1H), 7.56 (s, 2H), 7.35 (dd, *J* = 7.6, 1.8 Hz, 1H), 7.22 (ddd, *J* = 9.5, 7.4, 1.9 Hz, 2H), 7.05 (dd, *J* = 8.9, 2.5 Hz, 1H), 6.88 (d, *J* = 2.4 Hz, 1H), 5.50 (s, 1H), 5.22 (s, 2H), 3.76 (s, 2H), 3.17 (s, 2H), 3.12 (s, 2H), 2.70 (s, 2H), 2.21 (s, 2H); ¹³C NMR (75 MHz, CDCl₃) δ 176.94, 162.41, 158.08, 152.82, 139.81, 135.86, 134.23, 133.64, 130.70, 129.37, 128.13, 127.65, 127.45, 126.66, 125.76, 125.71, 122.13, 121.44, 118.26, 114.71, 101.26, 69.52, 58.70, 52.76, 49.90, 32.04, 29.06. MS(ESI) *m/z*: 540.2 [M + H]⁺.

(E)-3-((1-(2-bromobenzyl)-1,2,3,6-tetrahydropyridin-4-yl)methylene)-7-((4-(trifluoromethyl)benzyl)oxy)chroman-4-one (**D3**). White solid, yield 35.6%. mp:107-108°C. ¹H NMR (300 MHz, Chloroform-*d*) δ 8.14 (d, *J* = 8.9 Hz, 1H), 7.68 (d, *J* = 6.2 Hz, 2H), 7.65 (s, 1H), 7.57 (s, 1H), 7.56 – 7.51 (m, 2H), 7.51 – 7.48 (m, 1H), 7.29 –

7.24 (m, 1H), 7.09 (td, $J = 7.6, 1.8$ Hz, 1H), 7.02 (dd, $J = 8.9, 2.4$ Hz, 1H), 6.85 (d, $J = 2.4$ Hz, 1H), 5.48 (dt, $J = 3.6, 2.0$ Hz, 1H), 5.20 (s, 2H), 3.70 (s, 2H), 3.15 (s, 2H), 3.12 – 3.03 (m, 2H), 2.66 (t, $J = 5.7$ Hz, 2H), 2.16 (d, $J = 6.4$ Hz, 2H); ^{13}C NMR (75 MHz, CDCl_3) δ 176.9, 162.4, 158.0, 152.8, 139.8, 139.7, 137.5, 133.6, 132.6, 130.7, 130.6, 128.4, 127.6, 125.8, 125.7, 125.6, 124.5, 122.1, 121.4, 118.2, 114.7, 101.2, 69.5, 61.2, 52.7, 49.9, 32.0, 29.0. MS(ESI) m/z : 584.1 $[\text{M} + \text{H}]^+$.

(E)-3-((1-(2-methylbenzyl)-1,2,3,6-tetrahydropyridin-4-yl)methylene)-7-((4-(trifluoromethyl)benzyl)oxy)chroman-4-one (**D4**). White solid, yield 34.3%. mp: 111-112°C. ^1H NMR (300 MHz, Chloroform-*d*) δ 8.13 (d, $J = 8.9$ Hz, 1H), 7.76 (s, 1H), 7.66 (d, $J = 8.2$ Hz, 2H), 7.56 (d, $J = 8.0$ Hz, 2H), 7.43 (s, 1H), 7.17 (dd, $J = 6.1, 2.9$ Hz, 3H), 7.03 (dd, $J = 8.9, 2.4$ Hz, 1H), 6.87 (d, $J = 2.4$ Hz, 1H), 5.46 (s, 1H), 5.20 (s, 2H), 3.70 (s, 2H), 3.16 (s, 2H), 3.13 (s, 2H), 2.74 (s, 2H), 2.36 (s, 3H), 2.26 (d, $J = 15.2$ Hz, 2H); ^{13}C NMR (75 MHz, Chloroform-*d*) δ 176.96, 162.48, 158.13, 153.14, 139.77, 137.50, 134.00, 131.35, 130.73, 130.57, 130.30, 128.00, 127.53, 127.47, 126.08, 125.76, 125.71, 121.68, 119.57, 118.15, 114.86, 101.27, 69.54, 58.51, 51.66, 49.33, 32.10, 29.72, 19.55. MS(ESI) m/z : 520.2 $[\text{M} + \text{H}]^+$.

(E)-3-((1-(2-nitrobenzyl)-1,2,3,6-tetrahydropyridin-4-yl)methylene)-7-((4-(trifluoromethyl)benzyl)oxy)chroman-4-one (**D5**). White solid, yield 40.2%. mp: 103-106°C. ^1H NMR (400 MHz, Chloroform-*d*) δ 8.17 (d, $J = 8.9$ Hz, 1H), 7.85 (dd, $J = 8.1, 1.3$ Hz, 1H), 7.69 (q, $J = 3.7$ Hz, 4H), 7.59 (d, $J = 8.2$ Hz, 2H), 7.54 (dd, $J = 7.6, 1.3$ Hz, 1H), 7.40 (td, $J = 7.7, 1.5$ Hz, 1H), 7.06 (dd, $J = 8.9, 2.4$ Hz, 1H), 6.89 (d, $J = 2.4$ Hz, 1H), 5.48 (d, $J = 3.4$ Hz, 1H), 5.23 (s, 2H), 3.87 (s, 2H), 3.16 (s, 2H), 3.08 – 2.83 (m, 2H), 2.56 (t, $J = 5.6$ Hz, 2H), 2.13 (q, $J = 4.7, 4.2$ Hz, 2H); ^{13}C NMR (75 MHz, Chloroform-*d*) δ 177.04, 162.42, 158.11, 152.90, 149.63, 139.80, 134.29, 133.56, 132.64, 130.81, 127.73 (d, $J = 10.8$ Hz), 127.49, 125.80, 124.43, 122.11, 121.47, 118.23, 114.78, 101.24, 69.54, 58.49, 52.92, 49.96, 32.08, 29.12. MS(ESI) m/z : 551.2 $[\text{M} + \text{H}]^+$.

(E)-3-((1-(2-(trifluoromethyl)benzyl)-1,2,3,6-tetrahydropyridin-4-yl)methylene)-7-((4-(trifluoromethyl)benzyl)oxy)chroman-4-one (**D6**). White solid, yield 56.2%. mp:104-105°C. ¹H NMR (400 MHz, Chloroform-*d*) δ 8.16 (d, *J* = 8.8 Hz, 1H), 7.82 (d, *J* = 7.6 Hz, 1H), 7.69 (d, *J* = 3.9 Hz, 2H), 7.66 (s, 1H), 7.61 (d, *J* = 7.9 Hz, 1H), 7.56 (d, *J* = 8.1 Hz, 2H), 7.49 (d, *J* = 7.6 Hz, 1H), 7.31 (t, *J* = 7.7 Hz, 1H), 7.04 (dd, *J* = 8.9, 2.4 Hz, 1H), 6.87 (d, *J* = 2.4 Hz, 1H), 5.65 – 5.42 (m, 1H), 5.21 (s, 2H), 3.73 (s, 2H), 3.16 (s, 2H), 3.03 (d, *J* = 3.4 Hz, 2H), 2.58 (t, *J* = 5.7 Hz, 2H), 2.15 (d, *J* = 12.4 Hz, 2H); ¹³C NMR (75 MHz, CDCl₃) δ 176.9, 162.4, 158.0, 152.7, 139.7, 138.0, 133.6, 131.8, 130.1, 127.6, 127.4, 126.6, 125.7, 122.1, 121.5, 118.2, 114.7, 101.2, 69.5, 57.7, 53.0, 50.0, 32.0, 29.2. MS(ESI) *m/z*: 574.2 [M + H]⁺.

(E)-3-((1-(3-fluorobenzyl)-1,2,3,6-tetrahydropyridin-4-yl)methylene)-7-((4-(trifluoromethyl)benzyl)oxy)chroman-4-one (**D7**). White solid, yield 44.6%. mp:91-92°C. ¹H NMR (300 MHz, Chloroform-*d*) δ 8.15 (d, *J* = 8.9 Hz, 1H), 7.69 (d, *J* = 3.8 Hz, 2H), 7.66 (s, 1H), 7.56 (d, *J* = 8.1 Hz, 2H), 7.26 (s, 1H), 7.13 – 7.10 (m, 1H), 7.07 (t, *J* = 2.2 Hz, 1H), 7.04 (dd, *J* = 8.9, 2.4 Hz, 1H), 6.94 (d, *J* = 1.6 Hz, 1H), 6.86 (d, *J* = 2.4 Hz, 1H), 5.47 (s, 1H), 5.21 (s, 2H), 3.59 (s, 2H), 3.15 (s, 2H), 3.00 (s, 2H), 2.59 (t, *J* = 5.8 Hz, 2H), 2.17 (s, 2H); ¹³C NMR (75 MHz, CDCl₃) δ 176.9, 164.5, 162.4, 158.0, 152.8, 141.1, 139.8, 133.7, 129.6, 129.5, 127.6, 127.4, 125.7, 125.7, 124.5, 122.1, 121.2, 118.2, 115.9, 115.6, 114.7, 114.0, 113.8, 101.2, 69.5, 62.0, 52.7, 49.8, 32.0, 29.0. MS(ESI) *m/z*: 524.2 [M + H]⁺.

(E)-3-((1-(4-fluorobenzyl)-1,2,3,6-tetrahydropyridin-4-yl)methylene)-7-((4-(trifluoromethyl)benzyl)oxy)chroman-4-one (**D8**). White solid, yield 48.9%. mp:97-99°C. ¹H NMR (300 MHz, Chloroform-*d*) δ 8.14 (d, *J* = 8.9 Hz, 1H), 7.69 (d, *J* = 4.3 Hz, 2H), 7.66 (s, 1H), 7.56 (d, *J* = 8.1 Hz, 2H), 7.32 (dd, *J* = 8.4, 5.6 Hz, 2H), 7.05 (d, *J* = 2.4 Hz, 1H), 7.03 – 7.01 (m, 1H), 6.98 (d, *J* = 8.7 Hz, 1H), 6.86 (d, *J* = 2.4 Hz, 1H), 5.47 (d, *J* = 3.0 Hz, 1H), 5.21 (s, 2H), 3.57 (s, 2H), 3.15 (s, 2H), 2.99 (s, 2H), 2.60 (t, *J*

= 5.8 Hz, 2H), 2.17 (s, 2H); ¹³C NMR (75 MHz, Chloroform-*d*) δ 176.93, 162.46, 158.11, 152.95, 139.78, 133.98, 131.16, 130.84, 130.29, 127.61, 127.46, 125.78, 125.73, 121.89, 118.22, 115.38, 115.10, 114.79, 101.27, 69.54, 62.84, 52.11, 49.37, 32.05, 29.72. MS(ESI) *m/z*: 524.2 [M + H]⁺.

Biological evaluation. *AChE inhibition.* The potency of target compounds to inhibit AChE was tested using a slightly modified Ellman assay.⁵¹ To make an AChE solution (2U/mL), *electrophorus electricus* AChE (C3389, Sigma-Aldrich) was dissolved in 0.1 M phosphate buffer (pH 8.0). The 96-well plate was filled with 20 μL of phosphate buffer (pH 8.0), followed by adding different concentrations of test compounds (20 μL), 1 mM 5'-dithiobis (2-nitrobenzoic acid) (DTNB) solution (100 μL), and AChE solution (40 μL) respectively. 20 μL of acetylthiocholine iodide (1 mM) was added to the mixed solution after the plate was incubated for 15 minutes at 37°C. A microplate reader (Thermo Scientific) was used to immediately record the absorbance of each plate at 405 nm. The inhibition of each compound was calculated using the formula $(1 - A_i/A_c) \times 100$, where *A_i* and *A_c* represent the absorbance of AChE in the presence and absence of inhibitors, respectively. Each experiment was repeated three times. Using log concentration-percentage inhibition curves, the IC₅₀ values of all target compounds were graphically calculated (Graph Pad Prism 8.0).

MAO-B inhibition. Human MAO-B was purchased from Sigma-Aldrich (M7441). The capacity of the test compounds to inhibit MAO-B activity was assessed by Amplex Red MAO assay.³⁸ Briefly, 0.1 mL of sodium phosphate buffer (0.05 M, pH 7.4) containing the test compounds at various concentrations and adequate amounts of recombinant *h*MAO-B (0.75 μg/mL) was incubated for 15 min at 37°C in a 96-wells plate with flat and black bottom, which placed in a dark fluorimeter chamber. After this incubation period, the reaction was started by adding 200 μM (final concentrations) Amplex Red reagent (90101, Sigma-Aldrich), 1 U/mL horseradish peroxidase (P8375, Sigma-Aldrich), and 1 mM *p*-tyramine (T90344, Sigma-Aldrich). Based on the fluorescence

produced (excitation, 545 nm; emission, 590 nm), the results were quantified in a multi-detection microplate fluorescence reader (MD5, Thermo Scientific). Data were analyzed with GraphPad PRISM 8 utilizing implemented nonlinear regression fit "one-site competition" to determine the IC₅₀ values.

Kinetic characterization of AChE inhibition. The same modified Ellman assay was used to characterize the kinetics of AChE. In 96-well plates, three final concentrations of test compound **C10** (20 μL), 20 μL of acetylthiocholine iodide with different concentrations (1.5 - 4 mM), and 20 μL of PBS were added in each well, followed by 40 μL of AChE. 100 μL of 0.1 mM DTNB was added after 15 minutes of incubation at 37°C. A microplate reader (Thermo Scientific) was used to immediately record the absorbance of each plate at 405 nm. The plots were assessed using a weighted least squares analysis, in which the variance of V was assumed to be a constant percentage of the entire dataset V. The slope of these maps corresponds to the compound's concentration in a weighted analysis, and K_i was calculated as the ratio of the retest intercept to the retest slope.

Molecular docking study. Protein Data Bank (<https://www.rcsb.org>) was used to obtain the structures of AChE (PDB ID: 4EY7) and MAO-B (2V5Z). AChE and MAO-B were refined and the active pockets for AChE and MAO-B were defined using the protein preparation and receptor grid generation modules of Schrodinger software, respectively. Small molecules were refined using the ligand preparation module. Finally, small molecules were docked to AChE or MAO-B using the ligand docking module.

Cytotoxicity Assay on SH-SY5Y cells. Cytotoxicity assay on SH-SY5Y cells was performed as described in our previous study.⁴² SH-SY5Y cells were grown in a 25 cm² culture flask in fresh MEM/F12 medium containing 10% fetal bovine serum, 100 U/mL penicillin, and 100 g/mL streptomycin, and incubated at 37°C with 5% CO₂. In a 96-well plate, cells were seeded at a density of 110⁴ cells per well. The medium was removed after 24 hours of incubation. With serum-free media, compounds 10a or 13b (10, 20, 50 M) were prepared and added to each well of the plate for 24 hours. After a

24-hour treatment, each well received 10 mL of 3-(4,5-dimethyl-2-thiazolyl)-2,5-diphenyl-2-H-tetrazolium bromide. After 4 h of incubation at 37°C, 100 µL of DMSO were added to dissolve the formazan crystals, and the absorbance of the mixture was measured at 490 nm using a microplate reader (FC/K3, Thermo, Waltham, MA, USA). The survival rate was calculated using the formula A_e/A_b 100 percent, where A_e and A_b represent the absorbance of SH-SY5Y cells in the presence and absence of the tested drugs. Each experiment was carried out three times in total.

Determination of AChE activity in SH-SY5Y cells. The Ellman method was used to evaluate the effect of **C10** on inhibiting AChE. Ellman method is based on the reaction between thiocholine which is produced by AChE and chromogenic 5,5'-dithiobis-2-nitrobenzoic acid (DTNB) to measure the formation of the colorimetric product named 5-thio-2-nitrobenzoic acid (TNB) which is yellow. Cells were cultured in 96-well plates at a density of 1×10^5 cells/100 µL for 24 hours at 37°C with 5% CO₂. The cells were exposed to different concentrations of **C10** and donepezil for another 24 hours. After drug treatment, cell culture media was removed and 100 µL of lysis buffer was added into each well and left to incubate for 15 minutes at room temperature. After incubation, the media in each well was mixed well and 50 µL taken out and added into a new 96-well plate, and then 50 µL of acetylthiocholine reaction mixture (1 × DTNB stock solution, 1 × acetylthiocholine stock solution, 1 × assay buffer) added to each well. The samples, including the total 100 µL mixture, were then left to incubate for 30 minutes at room temperature. Acetylcholinesterase activity was measured using a TECAN plate reader at OD = 412nm. Data analyses were performed using the GraphPad Prism software. Activity values are plotted as a percentage of each group divided by the averaged of control, n=6.

Quantification of AChE-induced Aβ aggregation. A Thioflavin T (ThT) assay can be applied to test changes in fluorescence intensity of ThT when bound to amyloid fibrils. Aβ peptides treated by Hexafluoroisopropanol (HFIP) were dissolved in DMSO to reach a final 200 µM stock. The solubilized peptides were then centrifuged at 13500

rpm for 10 minutes. After centrifugation, the supernatant was transferred to a new vial for the following experiments. 2 μL of the test compound **C10** (at different desired concentration), 2 μL of 200 μM $\text{A}\beta$ peptides stock, 20 μL AChE enzyme and 76 μL of 1 \times PBS (pH 8.0) were added to each well of the 96-well plate. As for the control group, 2 μL of 200 μM $\text{A}\beta$ peptides stock were added into each well, followed by 20 μL AChE enzyme and 78 μL of 1 \times PBS (pH 8.0). As for the $\text{A}\beta$ only group, 2 μL of 200 μM $\text{A}\beta$ peptides stock and 98 μL of 1 \times PBS (pH 8.0) were added into each well. The reaction in all these groups was incubated for 24 hours at room temperature. 100 μL of 5 μM ThT was then added into each well and incubated for 1 hour at room temperature. After incubation, fluorescence emission was recorded using a Tecan Spark microplate reader (TECAN, Switzerland) at 490 nm with an excitation wavelength of 450 nm. Data analyses were performed using the GraphPad Prism software. Activity values are plotted as a percentage of each group divided by the averaged of control, n=6.

Measurement of Mitochondrial Membrane Potential (MMP). As a novel cationic dye, tetraethylbenzimidazolylcarbocyanine iodide (JC-1) accumulates in energized mitochondria. The dye is present as a monomer and yields green fluorescence when the MMP levels in cells are low. The dye aggregates in healthy cells with high MMP levels and emits an orange-red fluorescence. The MMP is important for maintaining cellular health and viability and decrease in a MMP level can increase the risk of apoptosis. MMPs were measured using a JC-1 assay kit. Cells (100 μL , 3×10^4 cells per well) were seeded into a 96-well plate and incubated for 24 hours at 37°C with 5% CO_2 . After 24-hour incubation, the cells were exposed to vehicle, donepezil or **C10** for 24 hours, and then treated with 30 nM okadaic acid (OA) for a further 24 hours. After treatment, cells were washed three times by PBS and then 2 μM of JC-1 dye was added and the cells were incubated for 30 minutes at 37°C with 5% CO_2 . The plate was then washed three times by dilution buffer solution. Finally, the plate was tested using a microplate reader (TECAN, Switzerland). Green fluorescence was measured at wavelengths of 485 nm excitation and 535 nm emission, while red fluorescence was measured at 535 nm excitation and 595 nm emission. Data analyses were performed using the GraphPad

Prism software. Activity values are plotted as a percentage of each group divided by the averaged of control, n=6.

Measurement of Intracellular ROS. 2',7'-dichlorofluorescein diacetate (DCFH-DA) fluorescence assay can be used to determine intracellular ROS levels. DCFH-DA itself is non-fluorescent and can freely go across the cell membrane. After entering the cell, DCFH-DA can be converted to dichlorofluorescein (DCFH) by intracellular esterase. DCFH is not permeable to the cell membrane, thus allowing the probe to be easily loaded into the cell. The ROS in the cell can oxidize non-fluorescent DCFH to generate fluorescent dichlorofluorescein (DCF) which can be utilized to quantify intracellular ROS level. 3×10^4 cells/100 μ L of cell suspension were seeded into a 96-well plate and cultured for 24 hours at 37°C with 5% CO₂. The cells were exposed to different concentrations of **C10** and donepezil for another 24 hours. After 24 hours drug treatment, cell culture media was removed and 30nM of okadaic acid (OA) were added into each well and left to incubate for 3 hours. After 3 hours incubation, cells were incubated with 20 μ M DCFH-DA for 30 minutes at 37°C with 5% CO₂. After 30 minutes, the dye was removed and the cells were washed three times with PBS. In the end, 100 μ L of fresh PBS was added to each well and fluorescence was measured using a microplate reader (TECAN, Switzerland). at wavelengths of 485 nm excitation and 535 nm emission.

Measurement of Tau Phosphorylation levels. SH-SY5Y cells were incubated in 6-well plates with a density of 3×10^5 cells/well. The **C10** and donepezil to be tested were co-incubated with glyceraldehyde (GA) for 24 h at 3 μ M and 0.3 μ M. Phosphorylated tau proteins were measured as follows: cells were dissolved in extraction buffer containing RIPA solution (1% Protease inhibitor and 1% phosphatase inhibitor), followed by incubation for 30min on ice. After being centrifuged (14000xg. 15min, 4°C), supernatants were applied to the ELISA kits KHB7041, KHB7031 and KHB0041 (ThermoFisher Scientific). Phosphorylation percentage was obtained, for the analyzed residues, by normalization against total tau.

Morris water maze test in scopolamine-induced mice. Experimental subjects were adult female ICR mice (8-10 weeks, 25-30 g, Shanghai, China). The mice were randomly divided into 4 groups on average (n = 8) : (i) control group (physiological saline); (ii) model group (scopolamine); (iii) compound group (scopolamine + C10 (10 mg/kg)); (iv) positive group (scopolamine + donepezil (10 mg/kg)). The 16-day experiment was split into the following sections: (1) Injection phase (days 1-10): donepezil (10 mg/kg), C10 (10 mg/kg) or saline were injected intraperitoneally once daily for 10 consecutive days, followed 30 min later by scopolamine solution (5 mg/kg). (2) Phase of exploration (days 11–16): The water maze was set up in a 25 °C, darkened space. A 10 cm diameter escape platform was placed in the center of the fourth quadrant of the circular pool, which had a 40 cm depth of water and a 120 cm diameter and 60 cm height. Each mouse underwent learning and memory training from days 11 through 14 and a cognitive behavioral test on days 16, all while receiving the same daily injections of the appropriate medications. After being dropped into the pool, the mice searched for the platform. From days 11 to 14, each mouse was trained once for 90 seconds in each of the pool's four quadrants, and the amount of time it took the mouse to locate the platform (i.e., make a successful escape) was recorded. The test was stopped by guiding the mice to the platform if they weren't able to get there in 90 seconds. Whether or not the mice managed to get to the platform in the allotted 90 seconds, they were kept there for 10 seconds. Mice were given 90 seconds to locate the platform in an exploratory experiment (water entry from the second quadrant) on the last day (day 16). Data on the time the mice reached the missing platform, the number of times they crossed the platform position and the escape latency was recorded by ANY-maze video tracking system and analyzed and processed using GraphPad Prism 8.0 software.

ASSOCIATED CONTENT

Supporting Information

The Supporting Information to this article can be found online.

ADMET parameter prediction of all compounds (Table S1), NMR spectra and

HPLC spectra of C1-C12 & D1-D8

Author Contributions

J.X., Z.Z. and H.Y. are responsible for the design of the study, acquiring funds, following up on progress, giving technical advice, compiling, editing, and revising the final manuscript. X.L. is responsible for design of new compounds, chemical synthesis and structural elucidation of most of the new compounds, as well as conducting molecular modeling studies, a part of the MAO-B and AChE assay and writing original draft. F.Z., J.L., Z.H., S.Z. and Y.J. completed part of the synthesis and the MAO-B and AChE assay. T.L., F.C., L.L., and B.Z. performed *in vitro* biological studies and *in vivo* cognitive impairment studies. All authors participated in writing the manuscript sections related to their experimental parts. All authors have read and approved the final form of the manuscript.

Notes

The authors declare that they have no known competing financial interests or personal relationships that could have appeared to influence the work reported in this paper.

ACKNOWLEDGMENTS

The authors thank the National Natural Science Foundation of China (No. 81874289) for financial support. This study was financed in part by the “Double First-Class” University project CPU2018GY04, China Pharmaceutical University, and partially by School of Pharmacy, The University of Nottingham.

REFERENCES

1. Wang, Y.; Sun, Y.; Guo, Y.; Wang, Z.; Huang, L.; Li, X. Dual functional cholinesterase and MAO inhibitors for the treatment of Alzheimer's disease: synthesis, pharmacological analysis and molecular modeling of homoisoflavonoid derivatives. *J. Enzyme Inhib. Med. Chem.* **2016**, *31* (3), 389-397.
2. Blennow, K.; de Leon, M. J.; Zetterberg, H. Alzheimer's disease. *Lancet* **2006**, *368* (9533), 387-403.

3. Goedert, M.; Spillantini, M. G. A century of Alzheimer's disease. *Science* **2006**, *314* (5800), 777-781.
4. Mucke, L. Neuroscience: Alzheimer's disease. *Nature* **2009**, *461* (7266), 895-897.
5. Bartus, R. T.; Dean, R. L., 3rd; Beer, B.; Lippa, A. S. The cholinergic hypothesis of geriatric memory dysfunction. *Science* **1982**, *217* (4558), 408-414.
6. Talesa, V. N. Acetylcholinesterase in Alzheimer's disease. *Mech. Ageing Dev.* **2001**, *122* (16), 1961-1969.
7. Hardy, J. A.; Higgins, G. A. Alzheimer's disease: the amyloid cascade hypothesis. *Science* **1992**, *256* (5054), 184-185.
8. Hardy, J.; Selkoe, D. J. The amyloid hypothesis of Alzheimer's disease: progress and problems on the road to therapeutics. *Science* **2002**, *297* (5580), 353-356.
9. Hardy, J. Alzheimer's disease: the amyloid cascade hypothesis: an update and reappraisal. *J. Alzheimers Dis.* **2006**, *9* (3 Suppl), 151-153.
10. Barnham, K. J.; Masters, C. L.; Bush, A. I. Neurodegenerative diseases and oxidative stress. *Nature reviews. Drug discovery* **2004**, *3* (3), 205-214.
11. Beal, M. F. Aging, energy, and oxidative stress in neurodegenerative diseases. *Ann. Neurol.* **1995**, *38* (3), 357-366.
12. Simonian, N. A.; Coyle, J. T. Oxidative stress in neurodegenerative diseases. *Annu. Rev. Pharmacol. Toxicol.* **1996**, *36*, 83-106.
13. Lin, M. T.; Beal, M. F. Mitochondrial dysfunction and oxidative stress in neurodegenerative diseases. *Nature* **2006**, *443* (7113), 787-795.
14. Grundke-Iqbal, I.; Iqbal, K.; Tung, Y. C.; Quinlan, M.; Wisniewski, H. M.; Binder, L. I. Abnormal phosphorylation of the microtubule-associated protein tau (tau) in Alzheimer cytoskeletal pathology. *Proc. Natl. Acad. Sci. U. S. A.* **1986**, *83* (13), 4913-4917.
15. Goedert, M.; Spillantini, M. G.; Jakes, R.; Rutherford, D.; Crowther, R. A. Multiple isoforms of human microtubule-associated protein tau: sequences and localization in neurofibrillary tangles of Alzheimer's disease. *Neuron* **1989**, *3* (4), 519-526.
16. Torres, J. M.; Lira, A. F.; Silva, D. R.; Guzzo, L. M.; Sant'Anna, C. M.; Kümmerle, A. E.; Rumjanek, V. M. Structural insights into cholinesterases inhibition

by harmane β -carbolinium derivatives: a kinetics-molecular modeling approach. *Phytochemistry* **2012**, *81*, 24-30.

17. Colombres, M.; Sagal, J. P.; Inestrosa, N. C. An overview of the current and novel drugs for Alzheimer's disease with particular reference to anti-cholinesterase compounds. *Curr. Pharm. Des.* **2004**, *10* (25), 3121-3130.

18. Contestabile, A. The history of the cholinergic hypothesis. *Behav. Brain Res.* **2011**, *221* (2), 334-340.

19. Sussman, J. L.; Harel, M.; Frolow, F.; Oefner, C.; Goldman, A.; Toker, L.; Silman, I. Atomic structure of acetylcholinesterase from *Torpedo californica*: a prototypic acetylcholine-binding protein. *Science* **1991**, *253* (5022), 872-879.

20. Inestrosa, N. C.; Alvarez, A.; Pérez, C. A.; Moreno, R. D.; Vicente, M.; Linker, C.; Casanueva, O. I.; Soto, C.; Garrido, J. Acetylcholinesterase accelerates assembly of amyloid-beta-peptides into Alzheimer's fibrils: possible role of the peripheral site of the enzyme. *Neuron* **1996**, *16* (4), 881-891.

21. Inestrosa, N. C.; Dinamarca, M. C.; Alvarez, A. Amyloid-cholinesterase interactions. Implications for Alzheimer's disease. *The FEBS journal* **2008**, *275* (4), 625-632.

22. Youdim, M. B.; Edmondson, D.; Tipton, K. F. The therapeutic potential of monoamine oxidase inhibitors. *Nat. Rev. Neurosci.* **2006**, *7* (4), 295-309.

23. Kumar, B.; Dwivedi, A. R.; Arora, T.; Raj, K.; Prashar, V.; Kumar, V.; Singh, S.; Prakash, J.; Kumar, V. Design, Synthesis, and Pharmacological Evaluation of N-Propargylated Diphenylpyrimidines as Multitarget Directed Ligands for the Treatment of Alzheimer's Disease. *ACS Chem. Neurosci.* **2022**, *13* (14), 2122-2139.

24. Mitoma, J.; Ito, A. Mitochondrial targeting signal of rat liver monoamine oxidase B is located at its carboxy terminus. *J. Biochem.* **1992**, *111* (1), 20-24.

25. Son, S. Y.; Ma, J.; Kondou, Y.; Yoshimura, M.; Yamashita, E.; Tsukihara, T. Structure of human monoamine oxidase A at 2.2-Å resolution: the control of opening the entry for substrates/inhibitors. *Proc. Natl. Acad. Sci. U. S. A.* **2008**, *105* (15), 5739-5744.

26. Binda, C.; Li, M.; Hubalek, F.; Restelli, N.; Edmondson, D. E.; Mattevi, A. Insights

- into the mode of inhibition of human mitochondrial monoamine oxidase B from high-resolution crystal structures. *Proc. Natl. Acad. Sci. U. S. A.* **2003**, *100* (17), 9750-9755.
27. Ramsay, R. R.; Sablin, S. O.; Singer, T. P. Redox properties of the flavin cofactor of monoamine oxidases A and B and their relationship to the kinetic mechanism. *Prog. Brain Res.* **1995**, *106*, 33-39.
28. Song, M. S.; Matveychuk, D.; MacKenzie, E. M.; Duchcherer, M.; Mousseau, D. D.; Baker, G. B. An update on amine oxidase inhibitors: multifaceted drugs. *Prog. Neuropsychopharmacol. Biol. Psychiatry* **2013**, *44*, 118-124.
29. Riederer, P.; Danielczyk, W.; Grünblatt, E. Monoamine oxidase-B inhibition in Alzheimer's disease. *Neurotoxicology* **2004**, *25* (1-2), 271-277.
30. Sterling, J.; Herzig, Y.; Goren, T.; Finkelstein, N.; Lerner, D.; Goldenberg, W.; Miskolczi, I.; Molnar, S.; Rantal, F.; Tamas, T.; Toth, G.; Zagyva, A.; Zekany, A.; Finberg, J.; Lavian, G.; Gross, A.; Friedman, R.; Razin, M.; Huang, W.; Kraus, B.; Chorev, M.; Youdim, M. B.; Weinstock, M. Novel dual inhibitors of AChE and MAO derived from hydroxy aminoindan and phenethylamine as potential treatment for Alzheimer's disease. *J. Med. Chem.* **2002**, *45* (24), 5260-5279.
31. Kamboj, S.; Singh, R. Chromanone-A Prerogative Therapeutic Scaffold: An Overview. *Arabian journal for science and engineering* **2022**, *47* (1), 75-111.
32. Alcaro, S.; Gaspar, A.; Ortuso, F.; Milhazes, N.; Orallo, F.; Uriarte, E.; Yáñez, M.; Borges, F. Chromone-2- and -3-carboxylic acids inhibit differently monoamine oxidases A and B. *Bioorg. Med. Chem. Lett.* **2010**, *20* (9), 2709-2712.
33. Gaspar, A.; Silva, T.; Yáñez, M.; Vina, D.; Orallo, F.; Ortuso, F.; Uriarte, E.; Alcaro, S.; Borges, F. Chromone, a privileged scaffold for the development of monoamine oxidase inhibitors. *J. Med. Chem.* **2011**, *54* (14), 5165-5173.
34. Legoabe, L. J.; Petzer, A.; Petzer, J. P. Selected chromone derivatives as inhibitors of monoamine oxidase. *Bioorg. Med. Chem. Lett.* **2012**, *22* (17), 5480-5484.
35. Legoabe, L. J.; Petzer, A.; Petzer, J. P., Selected C7-substituted chromone derivatives as monoamine oxidase inhibitors. *Bioorg. Chem.* **2012**, *45*, 1-11.
36. Legoabe, L. J.; Petzer, A.; Petzer, J. P. Inhibition of monoamine oxidase by selected C6-substituted chromone derivatives. *Eur. J. Med. Chem.* **2012**, *49*, 343-353.

37. Gnerre, C.; Catto, M.; Leonetti, F.; Weber, P.; Carrupt, P. A.; Altomare, C.; Carotti, A.; Testa, B. Inhibition of monoamine oxidases by functionalized coumarin derivatives: biological activities, QSARs, and 3D-QSARs. *J. Med. Chem.* **2000**, *43* (25), 4747-4758.
38. Lan, Jin.; Xie, S., Huang, Ming.; Hu, Ya.; Kong, L.; Wang, X. Chromanones: selective and reversible monoamine oxidase B inhibitors with nanomolar potency. *Med. Chem. Commun.* **2015**, *6* (7), 1293-1302.
39. Cloete, S. J.; N'Da, C. I.; Legoabe, L. J.; Petzer, A.; Petzer, J. P. The evaluation of 1-tetralone and 4-chromanone derivatives as inhibitors of monoamine oxidase. *Mol. Divers.* **2021**, *25* (1), 491-507.
40. Moutayakine, A.; Marques, C.; López, Ó.; Bagetta, D.; Leitzbach, L.; Hagenow, S.; Carreiro, E. P.; Stark, H.; Alcaro, S.; Fernández-Bolaños, J. G.; Burke, A. J. Evaluation of chromane derivatives: Promising privileged scaffolds for lead discovery within Alzheimer's disease. *Bioorg. Med. Chem.* **2022**, *68*, 116807.
41. de Beer, A. D.; Legoabe, L. J.; Petzer, A.; Petzer, J. P., The inhibition of catechol O-methyltransferase and monoamine oxidase by tetralone and indanone derivatives substituted with the nitrocatechol moiety. *Bioorg. Chem.* **2021**, *114*, 105130.
42. Li, X.; Jia, Y.; Li, J.; Zhang, P.; Li, T.; Lu, L.; Yao, H.; Liu, J.; Zhu, Z.; Xu, J. Novel and Potent Acetylcholinesterase Inhibitors for the Treatment of Alzheimer's Disease from Natural (\pm)-7,8-Dihydroxy-3-methyl-isochroman-4-one. *Molecules* **2022**, *27* (10).
43. Ellman, G. L.; Courtney, K. D.; Andres, V., Jr.; Feather-Stone, R. M. A new and rapid colorimetric determination of acetylcholinesterase activity. *Biochem. Pharmacol.* **1961**, *7*, 88-95.
44. Eldeen, I. M.; Elgorashi, E. E.; van Staden, J. Antibacterial, anti-inflammatory, anti-cholinesterase and mutagenic effects of extracts obtained from some trees used in South African traditional medicine. *J. Ethnopharmacol.* **2005**, *102* (3), 457-464.
45. Novaroli, L.; Reist, M.; Favre, E.; Carotti, A.; Catto, M.; Carrupt, P. A. Human recombinant monoamine oxidase B as reliable and efficient enzyme source for inhibitor screening. *Bioorg. Med. Chem.* **2005**, *13* (22), 6212-6217.
46. Dinamarca, M. C.; Arrázola, M.; Toledo, E.; Cerpa, W. F.; Hancke, J.; Inestrosa, N. C. Release of acetylcholinesterase (AChE) from beta-amyloid plaques assemblies

improves the spatial memory impairments in APP-transgenic mice. *Chem. Biol. Interact.* **2008**, *175* (1-3), 142-149.

47. Liu, Y.; Uras, G.; Onuwaje, I.; Li, W.; Yao, H.; Xu, S.; Li, X.; Li, X.; Phillips, J.; Allen, S.; Gong, Q.; Zhang, H.; Zhu, Z.; Liu, J.; Xu, J. Novel inhibitors of AChE and A β aggregation with neuroprotective properties as lead compounds for the treatment of Alzheimer's disease. *Eur. J. Med. Chem.* **2022**, *235*, 114305.

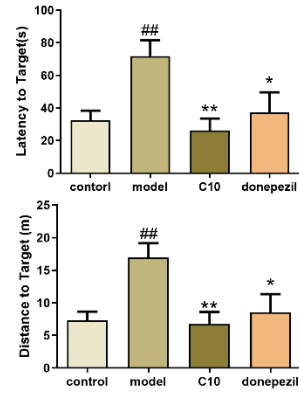
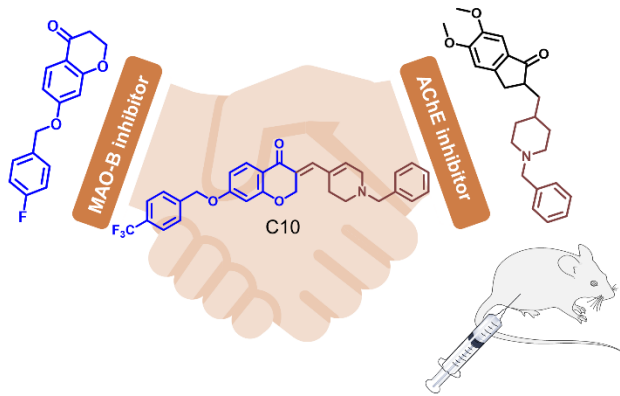
48. Yao, H.; Uras, G.; Zhang, P.; Xu, S.; Yin, Y.; Liu, J.; Qin, S.; Li, X.; Allen, S.; Bai, R.; Gong, Q.; Zhang, H.; Zhu, Z.; Xu, J. Discovery of Novel Tacrine-Pyrimidone Hybrids as Potent Dual AChE/GSK-3 Inhibitors for the Treatment of Alzheimer's Disease. *J. Med. Chem.* **2021**, *64* (11), 7483-7506.

49. Safer, D. J.; Allen, R. P. The central effects of scopolamine in man. *Biol. Psychiatry* **1971**, *3* (4), 347-355.

50. Klinkenberg, I.; Blokland, A., The validity of scopolamine as a pharmacological model for cognitive impairment: a review of animal behavioral studies. *Neurosci. Biobehav. Rev.* **2010**, *34* (8), 1307-1350.

51. Yang, X.; Qiang, X.; Li, Y.; Luo, L.; Xu, R.; Zheng, Y.; Cao, Z.; Tan, Z.; Deng, Y. Pyridoxine-resveratrol hybrids Mannich base derivatives as novel dual inhibitors of AChE and MAO-B with antioxidant and metal-chelating properties for the treatment of Alzheimer's disease. *Bioorg. Chem.* **2017**, *71*, 305-314.

GRAPHIC ABSTRACT



Potent inhibitory activity against AChE ✓

Improvement of cognition and memory of mice *in vivo* ✓

Potent inhibitory activity against MAO-B ✓

Neuroprotection and no cellular toxicity ✓

Inhibited AChE- induced A β aggregation ✓

Reduced GA-induced phosphorylation of tau ✓